

Perfect Fluids and Bad Metals: Transport Analogies Between Ultracold Fermi Gases and High T_c Superconductors

Hao Guo¹, Dan Wulin², Chih-Chun Chien³ and K. Levin²

¹*Department of Physics, University of Hong Kong, Hong Kong, China*

²*James Franck Institute and Department of Physics, University of Chicago, Chicago, Illinois 60637, USA and*

³*Theoretical Division, Los Alamos National Laboratory, MS B213, Los Alamos, NM 87545, USA*

(Dated: September 26, 2018)

In this paper, we examine in a unified fashion dissipative transport in strongly correlated systems. We thereby demonstrate the connection between “bad metals” (such as the high temperature superconductors) and “perfect fluids” (such as the ultracold Fermi gases, near unitarity). One motivation of this work is to communicate to the high energy physics community some of the central unsolved problems in high T_c superconductors. Because of interest in the nearly perfect fluidity of the cold gases and because of new tools such as the AdS/CFT correspondence, this better communication may lead to important progress in a variety of different fields. A second motivation is to draw attention to the great power of transport measurements which more directly reflect the excitation spectrum than, say, thermodynamics and thus strongly constrain microscopic theories of correlated fermionic superfluids. Our calculations show that bad metal and perfect fluid behavior is associated with the presence of a normal state excitation gap which suppresses the effective number of carriers leading to anomalously low conductivity and viscosity above the transition temperature T_c . Below T_c we demonstrate that the condensate collective modes (“phonons”) do not couple to transverse probes such as the shear viscosity. As a result, our calculated shear viscosity at low T becomes arbitrarily small as observed in experiments. In both homogeneous and trap calculations we do not find the upturn in η or η/s (where s is the entropy density) found in most theories. In the process of these studies we demonstrate compatibility with the transverse sum rule and find reasonable agreement with both viscosity and cuprate conductivity experiments.

PACS numbers: 03.75.Ss, 67.10.Jn, 67.85.De

I. INTRODUCTION

There is a widespread interest in studying ultracold Fermi gases to learn about some of the most strongly interacting systems in nature. It has been argued¹ that the atomic Fermi gas near unitarity provides a prototype for the physics of quark-gluon plasmas which are associated with the early stages of the Big Bang. Most remarkable about these two nominally different physical systems is the fact that they correspond to nearly perfect fluids, exhibiting even in their non-superfluid phases extremely small values of the shear viscosity η . In this paper we call attention to a third class of strongly interacting systems which is the metallic counterpart of the perfect (neutral) fluid, namely, the so-called “bad metal”². We show how low conductivity and low viscosity are analogous. Bad metals are known to exist in nature in a most fascinating class of materials: the high T_c superconductors. We argue here that to learn more about the physics of nearly perfect fluids it is particularly useful to study the behavior of the conductivity in the cuprate superconductors and vice versa. We note that it may seem at first sight paradoxical that bad metals and perfect fluids have anything in common since the condensate contribution to the conductivity is infinite in the metallic system whereas the viscosity counterpart in the neutral superfluid is zero. We stress throughout this paper that the dc transport (associated with $\omega \rightarrow 0$) in both cases reflects the normal fluid or *excitations* of the condensate.

Because the ultracold Fermi gases near the unitary limit are also thought to be related to quark-gluon plasmas¹, much attention has focused on particle-physics-based calculations of the anomalously low shear viscosity, η ^{3,4}. However, considerable insight into the thermodynamics⁵ and various spectroscopic studies^{6,7} has also been obtained via a condensed matter perspective. This paper belongs to the second school in which BCS theory is extended to accommodate arbitrarily strong interactions. We apply BCS to Bose Einstein condensation (BEC) crossover theory⁶ to compute η in the neutral Fermi gases and the conductivity σ (evaluated at $\omega \rightarrow 0$) for the charged counterparts, such as the high T_c superconductors. Our results, which are reasonably consistent with experiments, apply both above and below T_c . Essential to this work is demonstrable consistency with central sum rules and conservation laws⁸.

Experimentally this crossover can be straightforwardly observed in the ultracold Fermi gases by exploiting Feshbach resonances. As has been argued⁹, this crossover also appears relevant to the cuprates (i) because of their anomalously short coherence length. Added support comes from (ii) their anomalously high transition temperatures and (iii) the widespread effects of a normal state gap^{6,10}. (iv) The smooth evolution from over to underdoped behavior of the optical conductivity, has similarly been used to argue¹¹ that the BCS-BEC crossover scenario might be appropriate to the cuprates. Although the cold gases and high T_c cuprates have s and d -wave order parameters respectively, this difference does not significantly modify our treatment of transport.

The shear viscosity, like the dc conductivity, is a powerful probe for testing microscopic theories because it reflects the normal fluid component and is extremely sensitive to the nature of the excitation spectrum. The low T normal Fermi liquid phase with scattering lifetime γ^{-1} and effective mass m^* helps to set up the general nomenclature. Here $\eta = \frac{1}{5}nv_F^2\gamma^{-1}m^*$. Similarly $\sigma = \frac{ne^2}{m^*}\gamma^{-1}$. More generally, one can think of η and σ as characterized by the effective number of normal excitations ($n \rightarrow n_{eff}(T)$) as well as their lifetime which we emphasize here is a many body effect. Crucial is an understanding of how n_{eff} depends on T .

Our central conclusion is that both the effects of a fermionic gap (with onset temperature $T^* > T_c$) and non-condensed pairs act in concert to reduce n_{eff} and thus *lower* the shear viscosity and dc conductivity at all $T < T^*$. These non-condensed pairs are associated with the stronger than BCS attraction and are present for $0 < T < T^*$. When quantitatively compared with very recent shear viscosity experiments¹² (we independently infer¹³ an estimated lifetime from radio frequency data) the agreement is reasonable. We similarly compare the ($\omega \rightarrow 0$) dc conductivity (as well as its normal state $\omega \equiv 0$ inverse, $\sigma_{dc}^{-1}(T) = \rho(T)$, the resistivity) with the counterparts in the high T_c superconductors and find reasonable agreement with trends in doping and temperature. While condensed matter “simulations” based on these atomic Fermi gases are now of wide interest, our approach here is somewhat different because we focus on condensed matter phenomena which currently exist in nature, for example the pseudogap in the cuprate superconductors. We have emphasized the commonality for these two systems in past reviews⁶ and more recently⁷ in the context of analogous tools such as radio frequency spectroscopy, which is closely related to photoemission¹⁰. It seems natural then to investigate here the analogies in transport.

Our work is organized around a second important premise: any theory of transport or scattering in the superfluid Fermi gases (both above and below T_c) must be formulated in a fully gauge invariant and sum-rule consistent fashion. One could imagine doing more and more sophisticated many body theories than standard BCS-related approaches (i.e. summing more and more diagrams) but, if sum rules and conservation laws cannot be demonstrated to hold, we would argue the significance of these calculations is problematic. Indeed, a major theme of our recent^{14,15} work which is summarized in this overview is to arrive at a demonstrably consistent theory of this exotic superfluidity by extending the important contributions of Nambu¹⁶ to the case of BCS-BEC crossover. This will serve as a basis for computing gauge invariant and properly conserving response functions which are measured in transport and scattering experiments. It is not as straightforward to demonstrate this consistency in Monte Carlo or other numerically-based schemes. Moreover, as theories of BCS-BEC crossover become more and more diagrammatically complicated it is not straightforward to determine that they are compatible with gauge invariance and conservation laws. Once this compatibility is established the next step is to assess the physical implications of this consistency in experimental probes. We stress here that our approach to BCS-BEC crossover is semi-analytical and therefore reasonably transparent. Moreover, unlike alternative (more numerical diagrammatic schemes¹⁷) the normal to superfluid transition is properly smooth and second order.

A systematic treatment of transport in the Fermi superfluids requires the introduction¹⁸ of inter-dependent fermionic as well as bosonic (or pair) excitations. In past transport literature there has been a focus on either one¹⁹ or the other⁴, but not both. Here we use a Kubo-based formalism which readily accommodates the simultaneous bosonic and fermionic excitations of the normal state and condensate and thereby addresses n_{eff} quite accurately while the alternative Boltzmann or kinetic theory-based approaches do not naturally incorporate these multiple statistical effects. The Kubo approach includes scattering processes via the lifetimes²⁰ which appear in the various Green’s functions, while Boltzmann schemes treat lifetimes via collision integrals. However, because the physics of this dissipation is principally associated with the many body processes of boson-fermion inter-conversion (via a parameter γ which appears throughout this paper), it should be satisfactorily addressed only in theories which treat the mixed statistics.

We stress in this paper that dissipative transport in the normal phase must also be addressed if one is to fully understand the counterpart below T_c case. Except in strict BCS theory, this normal phase is affected by the below T_c pairing correlations. As a result, consistency checks need to be applied above T_c and the behavior must necessarily reflect that the transition is second order. Our central theme is based on the fact that the fermionic excitation gap or pairing gap persists above T_c as a “pseudogap” (except in strict BCS theory); this leads to important transport implications such as “nearly perfect fluidity” (reflecting anomalously small viscosity¹) or in the analogous charged system “bad metal”² behavior (reflecting anomalously small conductivity).

To add to the case for simultaneously studying both the viscosity and dc conductivity we note that the wealth of data available²¹ and the relative ease of measurement (compared to those in atomic or RHIC experiments) make the cuprates a particularly useful analogue for the nearly perfect fluids. In addition to dc measurements, one can probe²¹ the conductivity as a function of frequency ω , $\sigma_{ac}(\omega)$, over a wide range of ω . Because of the existence of a frequency sum rule, theories of the (dc) conductivity are thereby highly constrained. Importantly, this sum rule and an in depth understanding of the conductivity serve to constrain analogous microscopic theories of viscosity. Conventionally, “bad” metals are systems in which the estimated mean free path l is shorter than all length scales; along with anomalously low conductivity this leads to the absence of resistivity saturation. The descriptive “perfect” is also associated with a situation in which l is small compared to physical length scales²². In strongly correlated superfluids, we re-iterate here that small l does not solely reflect short transport lifetimes τ but rather a notable suppression in the effective “carrier number”. The influence of bad metallicity on superconductivity was studied in Ref. 2. Here we emphasize the converse: the influence of superconductivity on transport²³. Moreover, as will be discussed in more detail below, pairing fluctuations and the phase fluctuations invoked earlier² are clearly distinct.

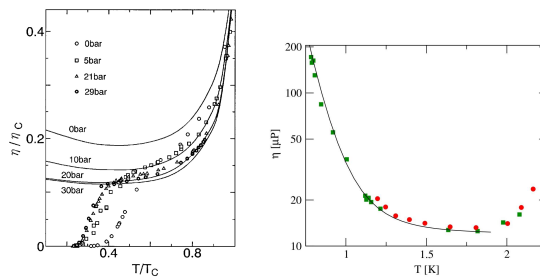


Figure 1: Viscosity in helium-3 (left) from Ref.28 and helium-4 from Ref.29 (right). The solid curves on the left represent theoretical predictions which were not verified. The viscosity vanishes for low temperature in the case of helium-3 because of a suppression of fermionic excitations. The behavior of η in helium-4 is governed by the rotons and phonons.

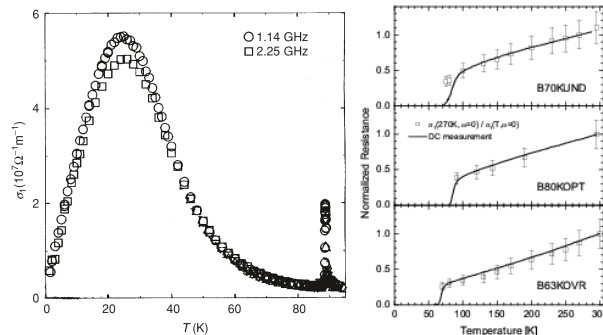


Figure 2: Temperature dependence of $\omega \rightarrow 0$ conductivity³⁰ (left) and resistivity³¹ (right) in the cuprates. The conductivity exhibits a maximum as a function of temperature because of competition between the effective carrier number and quasiparticle lifetime. Increasing the doping tends to lower the resistivity.

We have included a summary of the main results of this paper in Section I C. For ease in reading this paper, the reader who is not interested in the technical details can skip Sections II and III and go directly to Section IV.

A. Experimental Overview

To understand viscosity in fermionic superfluids, it is useful to begin with helium-3 which has been successfully described using BCS-based approaches, albeit for the p -wave case^{24,25}. Here experiments²⁶ indicate that η drops off rapidly to zero in the superfluid phase. This is shown in Figure 1 to the left. Interestingly, there is a minimum in η above T_c which is associated with strict Fermi liquid behavior²⁷. In a Fermi liquid the number of carriers and mass are both T independent, while the inter-fermion scattering lifetime varies as T^{-2} . The standard interpretation of the data below T_c is that η decreases with decreasing T as a result of the suppression of fermionic excitations at low T . In a strong magnetic field one spin component of the triplet is driven normal and this leads to a very different behavior for the shear viscosity²⁸, in which (even below T_c) it reflects the normal Fermi liquid behavior above T_c . In this A_1 phase, the low temperature behavior exhibits an upturn at low T ; this is not to be associated with coupling to collective modes or phonons, but rather reflects a residual normal component. In BCS-based superfluids, we stress¹⁶ that Nambu-Goldstone boson effects do not naturally enter into the transverse transport properties such as η . By contrast, in the helium-4 counterpart shown on the right in Fig. 1, the single particle bosonic excitations couple to the collective (Nambu-Goldstone) modes, leading to an upturn²⁹ in η at low T , which has also been predicted (but not seen) for the atomic Fermi superfluids⁴.

For strongly correlated charged systems, the counterpart experiments are summarized in Figure 2, here for the high T_c cuprates, which have d -wave pairing. On the left is the low T , $\omega \rightarrow 0$ conductivity for a $T_c \approx 90K$ sample. This shows the fairly generic maximum below T_c . The figure on the right is the resistivity or inverse conductivity for different stoichiometries as a function of temperature. Above T_c , two crucial points are that $\rho = \sigma^{-1}$ is nearly linear with T and its magnitude seems to decrease from the UND (underdoped) to the OVR (overdoped) samples. It is inferred³² from similar systematic studies that the effective number of carriers at fixed T is substantially depressed, varying as the doping x rather than the expected $1 + x$. Importantly, for the present purposes $\sigma(T)$ seems to approach zero at the lowest temperatures. The latter point is consistent with the vanishing η shown in the previous figure for the fermionic superfluid. The pronounced maximum is thought to arise from the

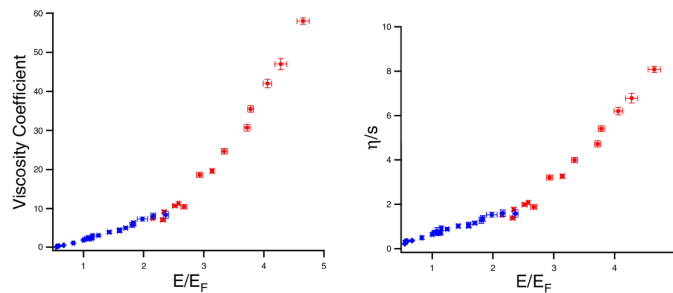


Figure 3: Viscosity experiments on unitary Fermi gases from recent experimental results showing the shear viscosity η and the ratio of viscosity and entropy density η/s , Ref.12. Importantly, the viscosity vanishes at low temperature and this puts a strong constraint on the theories of the unitary Fermi gas.

competition between the decrease in n_{eff} and the increase in the fermionic lifetime at low T . Such a competition is not nearly as apparent in an s -wave system where n_{eff} is exponentially suppressed.

In Fig. 3 we summarize recent viscosity experiments from the Duke group¹² on a unitary trapped Fermi gas. One sees here that despite previous predictions, the viscosity and its ratio to entropy density are both strongly suppressed at low T . We will return to all of these figures throughout the paper.

B. Theoretical Overview

The BCS-BEC crossover theory that is adopted here is based on a natural extension of the BCS ground state,

$$\Psi_0 = \prod_{\mathbf{k}} (u_{\mathbf{k}} + v_{\mathbf{k}} c_{\mathbf{k}\uparrow}^\dagger c_{-\mathbf{k}\downarrow}^\dagger) |0\rangle. \quad (1)$$

This ground state is often called the “BCS-Leggett” state. The observation that this state is much more general than originally presumed forms the basis for BCS-BEC crossover theory^{33–35}. To implement this generalization of the BCS ground state, all that is required is that one solve for the two variational parameters $u_{\mathbf{k}}$ and $v_{\mathbf{k}}$ in concert with a self consistent condition on the fermionic chemical potential μ . As the attraction is increased, μ becomes different from the Fermi energy E_F . The two variational parameters $u_{\mathbf{k}}$ and $v_{\mathbf{k}}$ can be converted to two more physically accessible parameters associated with the zero temperature gap (or equivalently order parameter) and μ . We stress that while in the cuprates the system is far from the BEC limit (in large part because of d -wave lattice effects³⁶), it is nevertheless quite distinct from the weak-coupling BCS limit due to the anomalously short coherence length⁹.

Since this wave function is so closely related to the BCS state, it is natural to ask whether its behavior away from $T = 0$ can be consolidated into as simple a formalism and physical picture as there is for the ground state. In Section II, we answer this question in the affirmative by recasting the equations of conventional BCS theory using a formalism that can then be readily generalized to include BCS-BEC crossover.

1. Simple Physical Picture of BCS-BEC Crossover Scenario

Before introducing the $T \neq 0$ formalism, we present a simple picture of the excitation spectra which ultimately enter into transport. The top row in Fig. 4 (from left to right) shows the schematic behavior as one passes from the $T = 0$ BCS-Leggett ground state to the above T^* Fermi liquid. The red (dotted circles) pairs are associated with net finite momentum, while the blue (solid circles) pairs correspond to the phase coherent condensate with zero center of mass momentum and the lone arrows represent fermionic excitations. The first panel shows that the ground state consists of fully condensed pairs [as in Eq. (1)], while the second panel shows that below T_c but above $T = 0$ there are both condensed and non-condensed pairs along with fermionic excitations. These non-condensed pairs persist above T_c (third panel) in the form of “preformed” pairs, while the condensed pairs are no longer present. Finally at temperatures above T^* all bosonic-like excitations are absent; the only excitations are fermionic. The second panel with $0 < T < T_c$ is the most interesting from the perspective of the present paper. In the cuprates, this is the regime in which the widely discussed³⁷ “two-gap” physics appears. Here the coexistence of the condensate and of non-condensed pairs, leads to two gap contributions³⁸, one associated with the pseudogap (called Δ_{pg}) and another associated with the condensate (called Δ_{sc}).

In contrast to this pairing fluctuation picture of the BCS-BEC crossover theory stands the phase fluctuation picture shown in the bottom row of Fig. 4. In this scenario of the pseudogap³⁹ there exist finite size regions of superconducting order in the normal

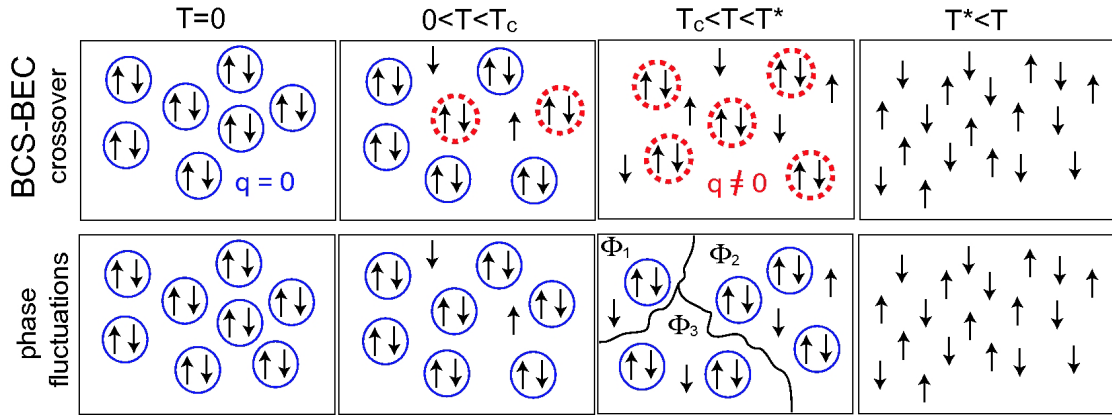


Figure 4: (Color online) Cartoon comparing the BCS-BEC crossover and phase fluctuation scenarios. Throughout, blue closed circles, lone arrows, and dashed red circles represent condensed fermion pairs, unpaired fermions, and finite lifetime pairs, respectively. The crossover theory is distinguished by the presence of noncondensed $\mathbf{q} \neq 0$ pairs for nonzero temperatures less than T^* . The defining feature of the phase fluctuation picture is the presence of different phase domains above T_c , indicated by the regions labelled with different Φ 's.

state. While the amplitude of the pairing gap $\Delta_{\mathbf{k}}$ is fixed in these regions, the superconducting phase, labeled by Φ , fluctuates spatially between them. The degree of phase fluctuation increases with temperature, and the Fermi liquid state is reached at $T > T^*$. In contrast, the phase is long-range ordered below T_c and the superconducting phase is described by the BCS state consisting only of condensed pairs and unpaired fermions. In this picture there appears as yet to be no counterpart to the “two gap physics” below T_c seen in the crossover scenario. In a simplified fashion, it could be said that the preformed pair theory is concerned with fluctuations in momentum space (in terms of $\mathbf{q} \neq 0$ pairing) while the phase fluctuation picture focuses on fluctuations of the phase in real space.

In the BCS-BEC crossover scenario, the effects of condensed [i.e., superconducting (sc)] and non-condensed [i.e., pseudo-gap (pg)] pairs are described by two distinct contributions to the fermionic self energy $\Sigma(\mathbf{k}, \omega)$

$$\Sigma(\mathbf{k}, \omega) = \Sigma_{pg, \mathbf{k}} + \Sigma_{sc, \mathbf{k}} = \frac{\Delta_{pg, \mathbf{k}}^2}{\omega + \xi_{\mathbf{k}} + i\gamma} + \frac{\Delta_{sc, \mathbf{k}}^2}{\omega + \xi_{\mathbf{k}}}. \quad (2)$$

The gap functions $\Delta_{pg, \mathbf{k}}$ and $\Delta_{sc, \mathbf{k}}$ are assumed to follow either a simple s or d -wave form. The condensed pairs have the usual BCS self energy contribution, Σ_{sc} , while the self energy of the non-condensed pairs Σ_{pg} possesses an additional term, γ , with γ^{-1} reflecting the finite lifetime of the non-condensed pairs. This form of Σ_{pg} was derived microscopically in Ref. 40 using a T -matrix approach (see below). It plays a central role in transport, largely through Ward identities which relate the self energy to transport properties. At the microscopic level, it is important to stress that the above expression for Σ_{pg} is not generic to all T -matrix theories, but strongly depends on an underlying BCS-like structure of the ground state associated with the present approach.

2. Lifetime Effects

In our discussion of dissipative transport, a crucial point is to address the origin of finite lifetime effects. Throughout this paper we will argue that *the central dissipation process is associated with the inter-conversion from fermions to pairs*. We stress that this is a many body effect and should not be associated with the two body scattering length. Nevertheless, at unitarity, these inter-conversion processes are likely to lead to the shortest lifetimes simply because the number of fermions and bosons is roughly equal there. This is in contrast to the BCS (BEC) regime in which there are virtually no bosons (fermions). This physical picture is consistent with Eq. (2) which above T_c has been rather widely adopted by the high T_c community^{41–43} and the cold Fermi gas community¹⁰. In this second context, it is this form of the fermionic self energy (or equivalently spectral function) which is to be associated with the downward dispersing quasi-particles revealed in momentum resolved radio frequency experiments^{7,44}. In the cuprates, above T_c , it is the finite lifetime of the non-condensed pairs which leads to the interesting physics associated with the “Fermi arcs”. These have been interpreted as a blurring of the d -wave nodes. Importantly, below T_c one sees their sudden collapse to conventional point nodes^{43,45} as a result of the onset of the order parameter Δ_{sc} .

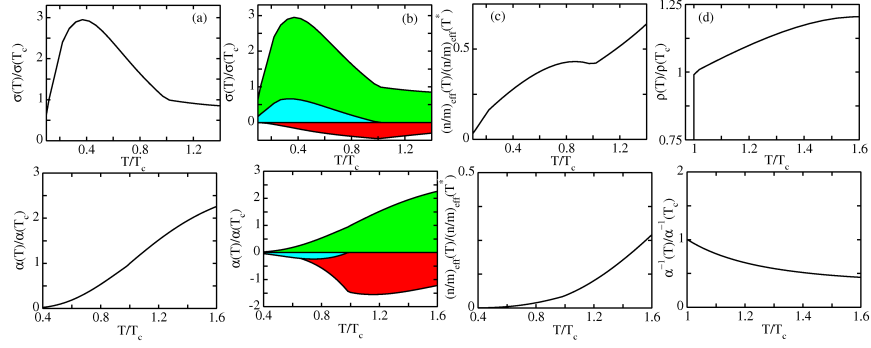


Figure 5: Summary figure of d -wave conductivity (top 4 panels) and s -wave viscosity (bottom 4 panels) as a function of temperature. Both panels (a) and the resistivity at the top in panel (d) (or inverse conductivity) can be compared with experiments in Figures 3 and 2. Panels (b) are contributions to transport from 3 components. Here red = pg, blue = sc, while green reflects the difference to make up the total. Panels (c) plot the effective carrier number and (d) the inverse transport coefficients.

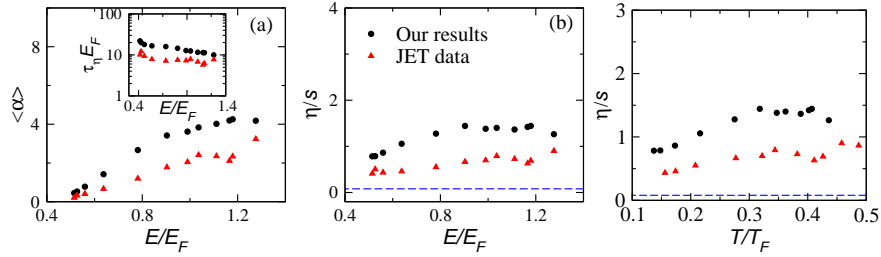


Figure 6: (a) Comparison of shear viscosity $\eta \equiv \alpha n \hbar$ and experiments⁴⁶ (red triangles) at unitarity for a trapped gas. In theory plots (black dots) we use the calculated thermodynamics for the trap energy E and entropy density s . The inset in (a) plots the estimated transport lifetime from radio frequency experiments¹³, as compared with the experimentally deduced lifetime needed for an exact fit to the theory. (b) Comparison of η/s . The blue dashed line labels the quantum lower limit of η/s given by string theory³. The last panel on the right converts the horizontal axis in (b) to temperature.

C. Central Results of this Paper

1. Summary of Central Formulae

In the weak dissipation limit (where γ is small), we may write down a combined expression for the shear viscosity and dc conductivity. We have

$$\left. \begin{array}{l} \eta \\ \sigma \end{array} \right\} = c_{\eta, \sigma} \int_0^{\infty} dp \frac{p^{6,4}}{m^2} \frac{E_{\mathbf{p}}^2 - \Delta_{pg}^2}{E_{\mathbf{p}}^2} (u_{\mathbf{p}}^2 \mp v_{\mathbf{p}}^2)^2 \left(-\frac{\partial f(E_{\mathbf{p}})}{\partial E_{\mathbf{p}}} \right) \tau_{\eta, \sigma} \quad (3)$$

Here $E_{\mathbf{p}}$ is the usual BCS dispersion, $E_{\mathbf{p}} \equiv \sqrt{\xi_{\mathbf{p}} + \Delta^2}$ where $\Delta^2 = \Delta_{pg}^2 + \Delta_{sc}^2$, and $f(E_{\mathbf{p}})$ is the Fermi function. We define $c_{\eta} = 1/15\pi^2$, $c_{\sigma} = 1/3\pi^2$ and the ‘‘coherence factors’’ are $u_{\mathbf{p}}^2, v_{\mathbf{p}}^2 = \frac{1}{2}(1 \pm \frac{\xi}{E})$. The transport lifetime $\tau_{\eta, \sigma}$ scales inversely with γ . This reduces to the usual BCS results when $\Delta_{pg}^2 = 0$. Eq. (3) contains two strong correlation effects which reduce the size of η and σ : the presence of a gap $\Delta(T)$ in E , which persists into the normal state and the presence of the factor $-\Delta_{pg}^2$ which reflects the reduction in the number of fermions contributing to dc transport as a result of their conversion to bosons. While the gap is fermionic in nature, this term is associated with bosonic degrees of freedom. In the stronger dissipation limit, the shear viscosity and conductivity can be rewritten in terms of generalized Green’s functions (to be defined more precisely in Sec. III).

$$\begin{aligned}
\eta &= -\lim_{\omega \rightarrow 0} \lim_{q \rightarrow 0} \frac{1}{\omega} \text{Im} \sum_P \frac{2p_x^2 p_y^2}{m^2} \left[G_{P^+} G_{P^-} - F_{sc,P^+} F_{sc,P^-} - F_{pg,P^+} F_{pg,P^-} - 2(u_{\mathbf{p}}^2 - v_{\mathbf{p}}^2)^2 F_{pg,P^+} F_{pg,P^-} \right]_{i\Omega_l \rightarrow \omega^+}, \\
\sigma &= -\lim_{\omega \rightarrow 0} \lim_{q \rightarrow 0} \frac{1}{\omega} \text{Im} \sum_P \frac{2p_z^2}{m^2} \left[G_{P^+} G_{P^-} + F_{sc,P^+} F_{sc,P^-} + F_{pg,P^+} F_{pg,P^-} - 2(u_{\mathbf{p}}^2 + v_{\mathbf{p}}^2)^2 F_{pg,P^+} F_{pg,P^-} \right]_{i\Omega_l \rightarrow \omega^+}, \quad (4)
\end{aligned}$$

where $P^+ = (i(\omega_n + \Omega_l), \mathbf{p} + \frac{\mathbf{q}}{2})$, $P^- = (i\omega_n, \mathbf{p} - \frac{\mathbf{q}}{2})$, and $\omega^+ = \omega + i0^+$. Note that while one can interpret F_{sc} as the usual Gor'kov Greens function reflecting superconducting order, there must also be a counterpart F_{pg} (discussed in detail later) which reflects non-condensed pairs. In previous work on both cold gases⁴⁷ and cuprates^{48,49} only the first term involving GG was included, and, moreover, this was correctly recognized^{47,49} as inadequate.

2. Summary of Transport Results

We next present summary numerical plots and compare the viscosity and d -wave conductivity calculations based on Eqs. (4). For definiteness we take a simple Fermi liquid $\gamma(T) \propto T^2$ temperature dependence for both transport properties. An essential change from s -wave to d -wave pairing is associated with the fact that for the latter the carrier number is no longer exponentially activated. As a consequence, the transport behavior tends to be more metallic.

The four top panels in Fig. 5 plot (a) the T_c -normalized, $\omega \rightarrow 0$, d -wave conductivity, $\text{Re}\sigma(T/T_c)$. In Fig. 5 (b) we plot a decomposition of this conductivity with three different contributions as color coded, so that the condensate (sc) is blue and the pg contributions are red, and what makes up the difference is shown in green.. Plotted in Fig.5(c) is the effective carrier number $(n/m(T))_{\text{eff}}$ which is obtained by multiplying σ by $\gamma(T)$ corresponding to the inverse lifetime. Finally in Figure 5(d) we plot the resistivity, or inverse conductivity, above T_c . The lower panel of figures corresponds to the counterpart plots for the s -wave viscosity, in terms of α defined via $\eta \equiv \alpha n \hbar$.

The figures in the (b) column show that the pg contributions are negative in both cases while the condensate gives a positive contribution to σ and a negative contribution for η ; this can be directly seen from Eqs. (4). The remainder (associated with the addition of the GG terms in Eqs. (4)), which yields the respective totals, is shown in green. That the (pg) contribution from the non-condensed pairs (red) lowers the conductivity and viscosity is because the presence of non-condensed pairs means fewer fermions are available for dc transport. Plotted in in the (c) column one sees that the effective carrier number $(n/m(T))_{\text{eff}}$ increases more or less monotonically as temperature is raised. This represents a generic figure, since here the temperature dependence of the lifetime has essentially been removed. Thus, this figure shows that the effective carrier number associated with the conductivity and its shear viscosity counterpart are increasing functions of temperature, *strongly suppressed by both the presence of a fermionic gap and the presence of bosonic degrees of freedom*. In Fig.5(d) we plot the inverse transport coefficients.

The first two figures (top and bottom) on the left in Fig.5 seem to capture the qualitative experimental transport features shown in Figures 2 for the cuprates and Figure 3 for the cold gases. The conductivity exhibits³⁰ a maximum below T_c , as can be seen experimentally from Fig.2, while the viscosity coefficient monotonically increases, as observed¹². As shown in panel (d), the conductivity of the normal state is appropriately metallic, but suppressed by the excitation gap. Importantly, the resistivity has a nearly linear temperature dependence as observed experimentally, in Fig. 2.

For the cold gases, more direct comparison with experiment involves inclusion of the trap. As is conventional⁶, we include trap effects via the local density approximation (LDA), or, equivalently Thomas-Fermi approximation. Figure 6 presents a comparison of the viscosity coefficient α between theory (based on the RF-deduced lifetime), as black dots, and experiment⁴⁶ (red triangles) as a function of E . These calculations can also be compared with more recent experiments summarized in Fig. 3. Our calculations, which predated the latest experimental data, will be discussed in more detail later. One can see, however, that the trends are compatible.

II. THEORETICAL FRAMEWORK OF BCS-BEC CROSSOVER

A. T-matrix Derivation of BCS Theory

In order to understand how to address BCS-BEC crossover at finite T , we now rederive standard BCS theory from a T-matrix scheme. Important here is that BCS theory can be viewed as incorporating *virtual* non-condensed pairs. Here we consider the general case applicable to both s and d -wave pairing by incorporating $\varphi_{\mathbf{k}} = [\cos(k_x) - \cos(k_y)]$ for the latter and taking it to be unity for the former. These virtual $Q \neq 0$ pairs are associated with an effective propagator or t-matrix which is constrained to

be of the form

$$t(Q) \equiv \frac{U}{1 + U \sum_K G_K G_{0,-K+Q} \varphi_{\mathbf{k}-\mathbf{q}/2}^2}. \quad (5)$$

in order to yield the standard BCS equations. This t-matrix is associated with a summation of ladder diagrams in the particle-particle channel [see Fig. 7 (a)] and importantly depends on both G and G_0 , which represent dressed and non-interacting Green's functions, respectively. We use K, Q to denote four-vectors with $K = (i\omega_n, \mathbf{k})$, $Q = (i\Omega_l, \mathbf{q})$, and where ω_n and Ω_l are fermion and boson Matsubara frequencies, respectively. In order to describe pairing in the $d_{x^2-y^2}$ -wave channel, we write the attractive fermion-fermion interaction in the form $U_{\mathbf{k},\mathbf{k}'} = U \varphi_{\mathbf{k}} \varphi_{\mathbf{k}'}$, where U is the strength of the pairing interaction. As in bosonic theories, non-condensed pair excitations of the condensate are necessarily gapless below T_c . This means that $t(Q \rightarrow 0) \rightarrow \infty$ which is equivalent to the vanishing of the effective pair chemical potential, $\mu_{pair} = 0$, for $T \leq T_c$. Thus we have a central constraint on the T -matrix

$$t^{-1}(Q \rightarrow 0) = 0 \rightarrow \mu_{pair} = 0, T \leq T_c \quad (6)$$

In order to show that the above condition is identical to the BCS gap equation, we need the appropriate form for G_K . In the BCS theory the fermionic self energy that appears in the fully dressed Green's function, G_K , is of the form

$$\Sigma_{sc,K} = \sum_Q t_{sc}(Q) G_{0,-K+Q} \varphi_{\mathbf{k}-\mathbf{q}/2}^2 = - \sum_Q \Delta_{sc,\mathbf{k}}^2 \delta(Q) G_{0,-K+Q} = -\Delta_{sc,\mathbf{k}}^2 G_{0,-K} \quad (7)$$

where $\Delta_{sc,\mathbf{k}}(T) \equiv \Delta_{sc}(T) \varphi_{\mathbf{k}}$ is the superconducting order parameter. The full Green's function is then obtained via the Dyson equation, $G_K = [G_{0,K}^{-1} - \Sigma_{sc,K}]^{-1}$, which, when inserted in Eq. (5) yields the BCS gap equation below T_c

$$1 = -U \sum_{\mathbf{k}} \frac{1 - 2f(E_{\mathbf{k}}^{sc})}{2E_{\mathbf{k}}^{sc}} \varphi_{\mathbf{k}}^2 \quad (8)$$

with $E_{\mathbf{k}}^{sc} \equiv \sqrt{\xi_{\mathbf{k}}^2 + \Delta_{sc,\mathbf{k}}^2}$. We have, thus, used Eqs. (5) and Eq. (6) to derive the standard BCS gap equation within a T -matrix language and the result appears in Eq. (8). Equation (6) above can be viewed as representing an extended version of the Thouless criterion of strict BCS which applies for all $T \leq T_c$. This derivation leads us to reaffirm the well known result⁵⁰⁻⁵² that BCS theory is associated with one bare and one dressed Green's function in the pair propagator.

B. Generalization to BCS-BEC crossover

To address BCS-BEC crossover, we presume that the non-condensed ($Q \neq 0$) pairs are no longer virtual. Thus the T-matrix of Eq. (5) in general possesses two contributions: the $\mathbf{q} = 0$ contribution that gives rise to the formation of the condensed or superconducting pairs and the $\mathbf{q} \neq 0$ contribution that describes the correlations associated with the non-condensed pairs. As a result, the fermionic self-energy also possesses two contributions which are given by

$$\Sigma(K) = \sum_Q t(Q) G_{0,-K+Q} \varphi_{\mathbf{k}-\mathbf{q}/2}^2 = \sum_Q [t_{sc}(Q) + t_{pg}(Q)] G_{0,-K+Q} \varphi_{\mathbf{k}-\mathbf{q}/2}^2 = \Sigma_{sc,K} + \Sigma_{pg,K} \quad (9)$$

The resulting full Green's function, $G^{-1} = G_0^{-1} - \Sigma_{sc} - \Sigma_{pg}$ is illustrated in Fig. 7(b). While as before, $\Sigma_{sc,K} = -\Delta_{sc,\mathbf{k}}^2 G_{0,-K}$, we find numerically^{53,54} that $\Sigma_{pg,K}$ is in general of the form

$$\Sigma_{pg,K} \approx \frac{\Delta_{pg,\mathbf{k}}^2}{\omega + \xi_{\mathbf{k}} + i\gamma} \quad (10)$$

with $\Delta_{pg,\mathbf{k}} = \Delta_{pg} \varphi_{\mathbf{k}}$. That is, the self-energy associated with the non-condensed pairs possesses the same structure as its BCS counterparts, albeit with a finite lifetime, γ^{-1} . Physically this arises from the fact that $t_{pg}(Q)$ is strongly peaked around $Q = 0$ below T_c where the pair chemical potential is zero and for a range of temperatures above T_c as well where this chemical potential is small.

Analytic self consistent equations for Δ_{pg} and Δ_{sc} can be obtained microscopically when we consider the small γ limit where

$$\Sigma(K) \approx -(\Delta_{sc,\mathbf{k}}^2 + \Delta_{pg,\mathbf{k}}^2) G_{0,-K} \equiv -\Delta_{\mathbf{k}}^2 G_{0,-K} \quad (11)$$

with

$$\Delta_{pg}^2 \equiv - \sum_Q t_{pg}(Q) \quad (12)$$

Here, we have used the fact that because of the vanishing of μ_{pair} below T_c , the bulk of the contribution to Σ_{pg} in the ordered state comes from small Q . This then leads to an effective pairing gap $\Delta(T)$ whose square is associated with the sum of the squares of the condensed and non-condensed contributions

$$\Delta_{\mathbf{k}}^2(T) = \Delta_{sc,\mathbf{k}}^2(T) + \Delta_{pg,\mathbf{k}}^2(T)$$

Note that the full gap $\Delta_{\mathbf{k}}$ remains relatively T-independent, even below T_c , as observed, because of the conversion of non-condensed ($\Delta_{pg,\mathbf{k}}$) to condensed ($\Delta_{sc,\mathbf{k}}$) pairs as the temperature is lowered.

The gap equation for this pairing gap, $\Delta_{\mathbf{k}}(T) = \Delta(T)\varphi_{\mathbf{k}}$, is again obtained from the condition $t_{pg}^{-1}(Q=0) = 0$, and given by

$$1 = -U \sum_{\mathbf{k}} \frac{1 - 2f(E_{\mathbf{k}})}{2E_{\mathbf{k}}} \varphi_{\mathbf{k}}^2, \quad (13)$$

This analysis can be made more explicit after analytical continuation so that⁴⁰, $t_{pg}(\omega, \mathbf{q}) \approx [Z(\Omega - \Omega_{\mathbf{q}}^0 + \mu_{pair}) + i\Gamma_Q]^{-1}$, where $Z = (\partial\chi/\partial\Omega)|_{\Omega=0, q=0}$, $\Omega_{\mathbf{q}}^0 \approx q^2/(2M_b)$ with the effective pair mass $M_b^{-1} = (1/2Z)(\partial^2\chi/\partial q^2)|_{\Omega=0, q=0}$. Near T_c , $\Gamma_Q \rightarrow 0$ faster than q^2 as $q \rightarrow 0$ and will be neglected. Then $\Delta_{pg}^2 \approx Z^{-1} \sum_{\mathbf{q}} b(\Omega_{\mathbf{q}}^0 - \mu_{pair})$.

Note that one needs to self-consistently determine the chemical potential, μ , by conserving the number of particles, $n = 2 \sum_K G_K$, which leads to

$$n = 2 \sum_K G_K = \sum_{\mathbf{k}} \left[1 - \frac{\xi_{\mathbf{k}}}{E_{\mathbf{k}}} + 2 \frac{\xi_{\mathbf{k}}}{E_{\mathbf{k}}} f(E_{\mathbf{k}}) \right] \quad (14)$$

Eqs. (12), (13), and (14) present a closed set of equations for the chemical potential μ , the pairing gap $\Delta_{\mathbf{k}}(T) = \Delta(T)\varphi_{\mathbf{k}}$, the pseudogap $\Delta_{pg,\mathbf{k}}(T) \equiv \Delta_{pg}(T)\varphi_{\mathbf{k}}$, and the superconducting order parameter $\Delta_{sc,\mathbf{k}}(T) = \Delta_{sc}\varphi_{\mathbf{k}}$ with $\Delta_{sc}(T) = \sqrt{\Delta^2(T) - \Delta_{pg}^2(T)}$. Following this approximation, $\Delta_{pg}(T)$ essentially vanishes in the ground state where $\Delta = \Delta_{sc}$. This is to be expected from the BCS-Leggett wavefunction in Eq. (1). In this way, the "two gap" physics disappears in the ground state. Importantly, numerical studies³⁶ show that for d -wave pairing, there is no superfluid phase in the bosonic regime where μ is negative; the pseudogap is, thus, associated with the fermionic regime.

III. TRANSPORT THEORY AND GAUGE INVARIANT APPROACHES TO SUPERCONDUCTIVITY AND SUPERFLUIDITY

Our transport theory for BCS-BEC crossover is based on linear response theory for both the density (or charge, labelled C) and spin (labelled S) degrees of freedom. In this approach, the U(1) electromagnetic (EM) gauge symmetry and the spin rotational symmetry around the z axis play important roles and an understanding of transport in strongly correlated superfluids has to incorporate in a central way the related conservation constraints. These enter via (i) the transverse f-sum rule. Application of the latter to the conductivity is, in turn, related to (ii) the absence (above T_c) and presence (below T_c) of a Meissner effect.

The perturbing Hamiltonian can be written in a compact form $\int d^3\mathbf{r} (\lambda_{\sigma,\sigma'}^{C,S} \psi_{\sigma}^{\dagger} \psi_{\sigma'} + \text{h.c.})$ where $\lambda_{\sigma,\sigma'}^{C,S} \propto \delta_{\sigma\sigma'}$ and $\lambda_{\sigma,\sigma'}^S \propto \delta_{\sigma\bar{\sigma}'}$. Here $\psi^{\dagger}(\psi)$ are the fermionic creation (annihilation) operators, $\sigma = \uparrow$ or \downarrow , $\uparrow = -\downarrow$ and $\bar{\sigma} = -\sigma$. We represent the density- density, current-current and spin correlation functions as, $\chi_{\rho\rho}$, $\overleftrightarrow{\chi}_{JJ}$ and χ_{SS} . Experimentally, the last of these three can be probed by spin-preserving and spin flip (two photon) Bragg scattering. The shear (η) and bulk viscosities (ζ_2) and the conductivity may be written in terms of the longitudinal (χ_L) and transverse (χ_T) components of the current-current correlation functions $\overleftrightarrow{\chi}_{JJ}$

$$\eta = -m^2 \lim_{\omega \rightarrow 0} \lim_{\mathbf{q} \rightarrow 0} \frac{\omega}{q^2} \text{Im} \chi_T(\omega, \mathbf{q}), \quad (15)$$

$$\zeta_2 + \frac{4}{3}\eta = -m^2 \lim_{\omega \rightarrow 0} \lim_{\mathbf{q} \rightarrow 0} \frac{\omega}{q^2} \text{Im} \chi_L(\mathbf{q}, \omega), \quad (16)$$

$$\sigma(\omega \rightarrow 0) = - \lim_{\omega \rightarrow 0} \lim_{q \rightarrow 0} \frac{\text{Im} \chi_T(\omega, \mathbf{q})}{\omega} \quad (17)$$

where the longitudinal $\chi_L = \hat{\mathbf{q}} \cdot \overleftrightarrow{\chi}_{JJ} \cdot \hat{\mathbf{q}}$ and transverse $\chi_T = (\sum_{\alpha=x}^z \chi_{JJ}^{\alpha\alpha} - \chi_L)/2$ susceptibilities satisfy⁸

$$\lim_{\mathbf{q} \rightarrow 0} \int_{-\infty}^{+\infty} \frac{d\omega}{\pi} \left(-\frac{\text{Im}\chi_T(\omega, \mathbf{q})}{\omega} \right) = \frac{n_n(T)}{m}, \quad (18)$$

$$\int_{-\infty}^{+\infty} \frac{d\omega}{\pi} \left(-\frac{\text{Im}\chi_L(\omega, \mathbf{q})}{\omega} \right) = \frac{n}{m}. \quad (19)$$

$$\int_{-\infty}^{\infty} d\Omega \text{Re}\sigma(\Omega) = e^2 \frac{n}{m} \quad (20)$$

Because we simultaneously discuss both neutral and charged systems, it is useful to define $e \equiv 1$ for the neutral case. Here n_n is the particle number of the normal component in the superfluid and the sum rules are explicitly written for the Fermi gas in which there are no bandstructure effects. For scattering probes, we define the associated structure factors for spin and charge or density in terms of closely related response functions, $\chi_{\rho\rho}$ and χ_{SS} :

$$S_C(\mathbf{q}, \omega) = -\frac{1}{\pi} \coth\left(\frac{\omega}{2T}\right) \text{Im}\chi_{\rho\rho}(\mathbf{q}, \omega) \quad \text{and} \quad S_S(\mathbf{q}, \omega) = -\frac{1}{\pi} \coth\left(\frac{\omega}{2T}\right) \text{Im}\chi_{SS}(\mathbf{q}, \omega)$$

Since the conservation laws for particle number and spin, $\partial^\mu J_\mu = 0$ and $\partial^\mu J_\mu^S = 0$ are satisfied, the following two sum rules must be respected at all temperatures in the whole BCS-BEC crossover regime:

$$\int_{-\infty}^{\infty} d\omega \omega S_{C,S}(\mathbf{q}, \omega) = \frac{n\mathbf{q}^2}{m} \quad \text{with} \quad \lim_{\mathbf{q} \rightarrow 0} S_{C,S}(\mathbf{q}, \omega) = 0. \quad (21)$$

The EM kernel is defined by $\mathbf{J} = -\overleftrightarrow{K} \cdot \mathbf{A}$, where $\overleftrightarrow{K}(Q) = e^2 (\overleftrightarrow{n}/m)_{dia} + \overleftrightarrow{P}(Q)$, and the paramagnetic contribution, given by $\overleftrightarrow{P}(Q)$, is associated with the normal current resulting from fermionic and bosonic excitations^{14,55}. In the superfluid phase, the density correlations which enter into scattering and the current correlations which enter into transport can be schematically written as a sum of 3 terms where for convenience we drop the (ω, \mathbf{q}) arguments: $\overleftrightarrow{\chi}_{JJ} = \overleftrightarrow{P} + \frac{\overleftrightarrow{n}}{m} + \overleftrightarrow{\text{Coll}}_J$ and $\chi_{\rho\rho} = P^{00} + \text{Coll}_\rho$. The counterparts for the spin degrees of freedom are $\overleftrightarrow{\chi}_{SS} = \overleftrightarrow{Q}_S + \frac{\overleftrightarrow{n}}{m}$ and $\chi_{SS} = Q_S^{00}$. Here \overleftrightarrow{P} , P^{00} and \overleftrightarrow{Q}_S , Q_S^{00} represent the ‘‘bare’’ contributions. Collective mode effects in the charge response, which are not present in the spin response, must also be included in the longitudinal response below T_c . These appear in the above equations as $\overleftrightarrow{\text{Coll}}_J$ and Coll_ρ . These collective mode effects are essential for insuring that the sum rules and related conservation laws are satisfied.

In the most general case, the diamagnetic current is expressed in terms of the inverse band mass $\partial^2 \xi_{\mathbf{k}} / \partial k_\alpha \partial k_\beta$ (with $\alpha, \beta = x, y, z$), via $(\overleftrightarrow{n}/m)_{dia} = 2 \sum_{K,\alpha} (\partial^2 \xi_{\mathbf{k}} / \partial \mathbf{k} \partial \mathbf{k}) G_K$. *Importantly, the latter contribution which is temperature independent, should not be confused with $(n/m(T))_{\text{eff}}$.* We stress that this effective carrier number is sensitive to the pairing gap $\Delta(T)$, while the diamagnetic contribution is not. We integrate the expression for the diamagnetic contribution by parts and use the self energy equation and the Generalized Ward identity to obtain (See Appendix A) an alternate form above T_c

$$\left(\frac{\overleftrightarrow{n}}{m}\right)_{dia} = -2 \sum_K \frac{\partial \xi_{\mathbf{k}}}{\partial \mathbf{k}} \frac{\partial \xi_{\mathbf{k}}}{\partial \mathbf{k}} \left[G_K^2 + \sum_P t_{pg}(P) G_{0,P-K}^2 G_K^2 \right] \quad (22)$$

This exact t-matrix based equation is significant because it has cast the diamagnetic response in the form of a two particle response function. That there is no Meissner effect in the normal state is related to a precise cancellation between the diamagnetic and paramagnetic terms. Noting $\overleftrightarrow{P}(0) = -e^2 (\overleftrightarrow{n}/m)_{dia}$, we may extend $\overleftrightarrow{P}(0)$ to finite Q to infer

$$\overleftrightarrow{P}(Q) = 2e^2 \sum_K \frac{\partial \xi_{\mathbf{k}+\mathbf{q}/2}}{\partial \mathbf{k}} \frac{\partial \xi_{\mathbf{k}+\mathbf{q}/2}}{\partial \mathbf{k}} \left[G_K G_{K+Q} + \sum_P t_{pg}(P) G_{0,P-K-Q} G_{0,P-K} G_{K+Q} G_K \right]. \quad (23)$$

Thus far, our discussion has been quite general, and we have circumvented any discussion of specific transport diagrams by building in the absence of a Meissner effect above T_c . One can alternatively^{14,55,56} introduce the Aslamazov-Larkin (AL) and Maki-Thompson (MT) diagrams to arrive at the above equation (see Fig 7), but the former which involves two factors of t_{pg} , at first sight, appears more complicated.

Collective mode effects are not present in the viscosity and conductivity, because they represent transverse probes. However, they play an important role in the density-density response. In this regard, it is convenient to define

$$S_\pm = (S_C \pm S_S)/2 \quad \text{from which it follows that} \quad \int_0^\infty d\omega \omega S_\pm(\omega, \mathbf{q}) = 0. \quad (24)$$

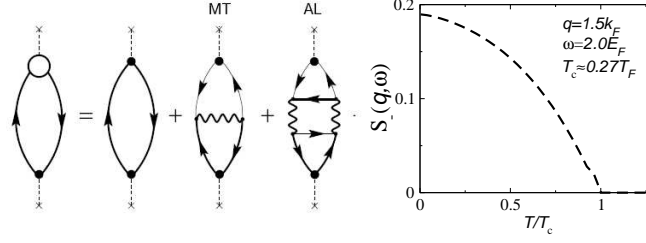


Figure 7: Characteristic diagrams which enter into the spin and charge response kernels (left). Heavy and light lines correspond to dressed and bare Green's functions. Here the wavy lines represent the pair propagator t . The corrections to the vertex include the Maki Thompson (MT) and Aslamazov-Larkin (AL) diagrams. Temperature dependence of $S_-(\mathbf{q})$ (see Eq. (24) in units of $n/2E_F$) for fixed momentum transfer $q = 1.5k_F$ and frequency $\omega = 2.0E_F$ at unitarity (right). This figure shows that S_- behaves like an order parameter¹⁴.

This latter is a very unusual sum rule. However, it *must* be satisfied in any consistent theory of superfluidity, providing spin and charge are conserved. In Appendix B we show how this sum rule is satisfied above T_c for an alternate BCS-BEC crossover theory introduced by Nozieres and Schmitt-Rink (NSR)³⁵.

There are other physical consequences which can be deduced once one has a conservation-law consistent theory. The conductivity and the shear viscosity can alternatively be written in terms of the bare response $P(Q)$ so that

$$\sigma(\omega) = -\lim_{\mathbf{q} \rightarrow 0} \frac{\text{Im}P^{xx}(\omega, \mathbf{q})}{\omega} \quad \text{with} \quad \eta = -m^2 \lim_{\omega \rightarrow 0} \lim_{\mathbf{q} \rightarrow 0} \frac{\omega}{q^2} \text{Im}P^{xx}(\omega, \mathbf{q}). \quad (25)$$

Moreover, in this way, one can see how closely related they are. We will not in this paper address the bulk viscosity, principally because we do not have the same level of theoretical control to satisfy the longitudinal f -sum rule, which is also more problematic below T_c , where the Goldstone bosons appear¹⁶.

A. Weak Dissipation Regime

In the previous section we have set up the general linearized response theory. We now discuss the detailed implementation of this formalism based on Eq. (2). Consistency with conservation laws requires that transport diagrams assume a specific form, reflecting the behavior of the self energy. We begin with the so-called “weak dissipation” regime, where in Eq. (2) we presume the quantity $\gamma \approx 0$. The strong dissipation regime is discussed in the next subsection. We have found that for the viscosity there is very little difference between weak and strong dissipation-based calculations, but this is not true for the d -wave conductivity, because of the easy excitations of fermions around the nodes. We indicate in Figure 7 the characteristic diagrams which enter into the generalized correlation functions. As a result one can show¹⁵ that the “bare” contributions to generalized charge and spin susceptibilities take on an extremely simple form

$$\left. \begin{aligned} P^{00}(\omega, \mathbf{q}) \\ Q_S^{00}(\omega, \mathbf{q}) \end{aligned} \right\} = \sum_{\mathbf{p}} \left[\frac{E_{\mathbf{p}}^+ + E_{\mathbf{p}}^-}{E_{\mathbf{p}}^+ E_{\mathbf{p}}^-} \frac{E_{\mathbf{p}}^+ E_{\mathbf{p}}^- - \xi_{\mathbf{p}}^+ \xi_{\mathbf{p}}^- \pm \Delta_{sc}^2 - \Delta_{pg}^2}{\omega^2 - (E_{\mathbf{p}}^+ + E_{\mathbf{p}}^-)^2} (1 - f(E_{\mathbf{p}}^+) - f(E_{\mathbf{p}}^-)) \right. \\ \left. - \frac{E_{\mathbf{p}}^+ - E_{\mathbf{p}}^-}{E_{\mathbf{p}}^+ E_{\mathbf{p}}^-} \frac{E_{\mathbf{p}}^+ E_{\mathbf{p}}^- + \xi_{\mathbf{p}}^+ \xi_{\mathbf{p}}^- \mp \Delta_{sc}^2 + \Delta_{pg}^2}{\omega^2 - (E_{\mathbf{p}}^+ - E_{\mathbf{p}}^-)^2} (f(E_{\mathbf{p}}^+) - f(E_{\mathbf{p}}^-)) \right], \quad (26)$$

$$\left. \begin{aligned} \overleftrightarrow{P}(\omega, \mathbf{q}) \\ \overleftrightarrow{Q}_S(\omega, \mathbf{q}) \end{aligned} \right\} = \sum_{\mathbf{p}} \frac{\mathbf{p} \cdot \mathbf{p}}{m \cdot m} \left[\frac{E_{\mathbf{p}}^+ + E_{\mathbf{p}}^-}{E_{\mathbf{p}}^+ E_{\mathbf{p}}^-} \frac{E_{\mathbf{p}}^+ E_{\mathbf{p}}^- - \xi_{\mathbf{p}}^+ \xi_{\mathbf{p}}^- \mp \Delta_{sc}^2 + \Delta_{pg}^2}{\omega^2 - (E_{\mathbf{p}}^+ + E_{\mathbf{p}}^-)^2} (1 - f(E_{\mathbf{p}}^+) - f(E_{\mathbf{p}}^-)) \right. \\ \left. - \frac{E_{\mathbf{p}}^+ - E_{\mathbf{p}}^-}{E_{\mathbf{p}}^+ E_{\mathbf{p}}^-} \frac{E_{\mathbf{p}}^+ E_{\mathbf{p}}^- + \xi_{\mathbf{p}}^+ \xi_{\mathbf{p}}^- \pm \Delta_{sc}^2 - \Delta_{pg}^2}{\omega^2 - (E_{\mathbf{p}}^+ - E_{\mathbf{p}}^-)^2} (f(E_{\mathbf{p}}^+) - f(E_{\mathbf{p}}^-)) \right]. \quad (27)$$

where ω implicitly has a small imaginary part and we define the quantities $E_{\mathbf{p}}^{\pm} = E_{\mathbf{p} \pm \mathbf{q}/2}$ and $\xi_{\mathbf{p}}^{\pm} = \xi_{\mathbf{p} \pm \mathbf{q}/2}$. Note that Eqs. (26) and (27) are exactly the same as their BCS counterparts when $\Delta_{pg}^2 \rightarrow 0$. It is quite remarkable that when we compare these two equations we see that the charge response functions reflect the difference $\Delta_{sc}^2 - \Delta_{pg}^2$ while the spin response functions depend on the total pairing gap $\Delta^2 = \Delta_{sc}^2 + \Delta_{pg}^2$. We may say that spin correlation functions know only about pairing whereas their charge counterparts reflect also coherent superfluid order.

From the definition of $\chi_T(\omega, \mathbf{q})$ the shear viscosity is given by

$$\eta = -m^2 \lim_{\omega \rightarrow 0} \lim_{\mathbf{q} \rightarrow 0} \frac{\pi\omega}{2q^2} \sum_{\mathbf{p}} \frac{p^2 \sin^2 \theta}{m^2} \left[(1 - f(E_{\mathbf{p}}^+) - f(E_{\mathbf{p}}^-)) \frac{E_{\mathbf{p}}^+ E_{\mathbf{p}}^- - \xi_{\mathbf{p}}^+ \xi_{\mathbf{p}}^- - \delta\Delta^2}{2E_{\mathbf{p}}^+ E_{\mathbf{p}}^-} (\delta_1(\omega) - \delta_1(-\omega)) \right. \\ \left. - (f(E_{\mathbf{p}}^+) - f(E_{\mathbf{p}}^-)) \frac{E_{\mathbf{p}}^+ E_{\mathbf{p}}^- + \xi_{\mathbf{p}}^+ \xi_{\mathbf{p}}^- + \delta\Delta^2}{2E_{\mathbf{p}}^+ E_{\mathbf{p}}^-} (\delta_2(\omega) - \delta_2(-\omega)) \right], \quad (28)$$

where we have used the abbreviated notation: $\delta_1(\omega) = \delta(\omega - E_{\mathbf{p}}^+ - E_{\mathbf{p}}^-)$, $\delta_2(\omega) = \delta(\omega - E_{\mathbf{p}}^+ + E_{\mathbf{p}}^-)$. Physically, two types of terms appear in the above equation. Both are well known in standard BCS theory. The first refers to processes which require a minimal frequency of the order of $2\Delta(T)$; they arise from the contribution of fermions which are effectively liberated by the breaking of pairs. The second of these terms, involving δ_2 , arises from scattering of fermionic quasi-particles and is the only surviving contribution to the viscosities, which are defined in the $\omega \rightarrow 0$ limit. Note that both contributions involve the *difference* of the condensed and non-condensed components ($\delta\Delta^2 = \Delta_{\text{sc}}^2 - \Delta_{\text{pg}}^2$) with opposite overall signs. The low ω quasi-particle scattering processes are reduced by the presence of non-condensed pairs – because they are associated with a reduction in the number of fermions. By contrast in the high $\omega \approx 2\Delta$ limit the number of contributing fermions will be increased by breaking pairs. We next take the low ω, q limits in Eq. (28) and introduce lifetime (or dissipation) effects by writing delta functions as Lorentzians $\delta(\omega \pm \mathbf{q} \cdot \nabla E_{\mathbf{p}}) \rightarrow \frac{1}{\pi} \frac{\gamma_{\eta}}{(\omega \pm \mathbf{q} \cdot \nabla E_{\mathbf{p}})^2 + \gamma_{\eta}^2}$. In this way we arrive at Eq. (3) which was presented in the summary section. Note that η assumes a form similar to a stress tensor- stress tensor correlation function.

The transport expressions summarized earlier in Eq. (3) correspond to the generally familiar BCS form^{24,25} except for the effects associated with non-zero Δ_{pg} which appears as a prefactor $1 - \frac{\Delta_{\text{pg}}^2}{E^2}$. This deviation from unity can be traced to the AL diagrams and hence may be interpreted as extra “bosonic” contributions which contribute to the normal fluid n_n . Their presence is physically required for the sum rule consistency of χ_T . Note that these terms enter with an overall reduction coherence-effect-prefactor associated with ξ^2/E^2 . The negative sign for this bosonic term comes from the fact that only fermions contribute directly to transport within a BCS-Leggett-based scheme; the more pairs which are present, the lower the fermionic contribution to the viscosity. We see from Eq. (4) that σ and η are alike except for momentum power law prefactors and coherence factors, When extended to finite frequency we note that unlike in BCS theory, there is a pair creation and pair-breaking contribution to the optical conductivity. This term is necessarily absent in a clean BCS superconductor, but may well be the origin of the widely observed²¹ “mid-infrared” contribution to the finite ω conductivity.

B. Explicit Proof of the transverse f Sum Rule

An important check on our microscopic scheme is to show that it satisfies the sum rule for the transverse component. The sum rule which are going to prove is in Eq. (18). Our proof here is explicitly for the weak dissipation form of the response functions and for the Fermi gas, where there are no bandstructure effects. We generalize this later in the paper.

The total particle number is

$$n = \sum_{\mathbf{p}} \left(1 - \frac{\xi_{\mathbf{p}}}{E_{\mathbf{p}}} (1 - 2f(E_{\mathbf{p}})) \right) = \frac{2}{m} \sum_{\mathbf{p}} \frac{p^2}{3E_{\mathbf{p}}^2} \left(\frac{1 - 2f(E_{\mathbf{p}})}{2E_{\mathbf{p}}} \Delta^2 - \xi_{\mathbf{p}}^2 \frac{\partial f(E_{\mathbf{p}})}{\partial E_{\mathbf{p}}} \right). \quad (29)$$

The superfluid density at general temperature³⁸ is given by

$$n_s = \frac{2}{3} \frac{\Delta_{\text{sc}}^2}{m} \sum_{\mathbf{p}} \frac{p^2}{E_{\mathbf{p}}^2} \left(\frac{1 - 2f(E_{\mathbf{p}})}{2E_{\mathbf{p}}} + \frac{\partial f(E_{\mathbf{p}})}{\partial E_{\mathbf{p}}} \right). \quad (30)$$

Therefore

$$n_n = n - n_s = \frac{2}{3} \sum_{\mathbf{p}} \frac{p^2}{E_{\mathbf{p}}^2} \left(\frac{\Delta_{\text{pg}}^2}{m} \frac{1 - 2f(E_{\mathbf{p}})}{2E_{\mathbf{p}}} - \frac{E_{\mathbf{p}}^2 - \Delta_{\text{pg}}^2}{m} \frac{\partial f(E_{\mathbf{p}})}{\partial E_{\mathbf{p}}} \right). \quad (31)$$

Using $\overleftrightarrow{\chi}_{JJ} = \overleftrightarrow{P} + \frac{\overleftrightarrow{n}}{m}$ leads to

$$\lim_{q \rightarrow 0} \int_{-\infty}^{+\infty} \frac{d\omega}{\pi} \left(-\frac{\text{Im}\chi_T}{\omega} \right) = \frac{2}{3m} \sum_{\mathbf{p}} \frac{p^2}{E_{\mathbf{p}}^2} \left(\frac{\Delta_{\text{pg}}^2}{m} \frac{1 - 2f(E_{\mathbf{p}})}{2E_{\mathbf{p}}} - \frac{E_{\mathbf{p}}^2 - \Delta_{\text{pg}}^2}{m} \frac{\partial f(E_{\mathbf{p}})}{\partial E_{\mathbf{p}}} \right) = \frac{n_n}{m}. \quad (32)$$

By contrast, (except in special cases, such as $q \rightarrow 0$, above T_c), the longitudinal sum rule requires numerical proof. Following the analysis in Ref. 14 we find agreement with the sum rule to within 5-10%. In addition to sum rule consistency, the appropriate diagram set for computing all transport properties must be chosen so that $n_s(T)$ vanishes at and above T_c . This is somewhat more complicated⁵⁷ to ensure than in strict BCS theory because there is a finite excitation gap at the transition. This gap or pseudogap, in turn, reflects the fact that there are bosonic excitations in addition to the fermions which deplete the condensate. In Section III E we present a more general argument for establishing the conductivity sum rule whether the dissipation is weak or strong.

C. Two Photon Bragg Experiments

In a recent paper¹⁴ we have used this theory to address the dynamical structure factor and thereby show how two photon Bragg scattering can be used to establish *in situ* the presence of coherent order in a superfluid, at any temperature, wavevector and frequency. For the most part experiments on unitary gases have relied on sweeps to the BEC, to find evidence for condensation. Our analysis is based on the definitions and sum rule in Eq. (24). It, thus, depends on imposing the current conservation laws, which have been extensively studied and verified¹⁴. Using the characteristic diagrams shown in Figure 7, which enter into the density-density correlation functions *we are now led to an important observation: the quantity $S_-(\omega, \mathbf{q})$ for all $\mathbf{q}, \omega, \mathbf{1}/\mathbf{k}_F \mathbf{a}$ can be used as an indication of in-situ superfluid order, without requiring sweeps to the BEC.* We show a plot of this behavior in the right-hand panel of Figure 7, where it can be seen that the difference structure factor vanishes in the normal state. An interpretation of this figure is that despite previous claims⁵⁸ *there is no spin-charge separation in the normal or pseudogap state associated with BCS-BEC crossover.* Spin-charge separation is, however, to be found in the superfluid phase. The counterpart normal state calculations can be shown to be valid in an alternate BCS-BEC crossover theory, based on the Nozieres Schmitt-Rink scheme³⁵; this is presented in Appendix B.

D. Strong Dissipation Approach

We now use the full expression for the self energy Eq. (2) to obtain compatible expressions for transport coefficients The full Green's function is given by

$$G_K = \left(i\omega_n - \xi_{\mathbf{k}} + i\gamma - \frac{\Delta_{pg,\mathbf{k}}^2}{i\omega_n + \xi_{\mathbf{k}} + i\gamma} - \frac{\Delta_{sc,\mathbf{k}}^2}{i\omega_n + \xi_{\mathbf{k}}} \right)^{-1}. \quad (33)$$

where we have added an extra constant term $i\gamma$ in order to be consistent with the weak dissipation limit in the case that γ becomes small. To extend $\overleftrightarrow{P}(Q)$ which appears in Eq. (23) below T_c , within a BCS-like formulation one needs to include terms of the form $F_{sc,K} F_{sc,K+Q}$ which represent the usual Gor'kov functions as a product of one dressed and one bare Green's function (GG_0)

$$F_{sc,K} \equiv -\frac{\Delta_{sc,\mathbf{k}}}{i\omega_n + \xi_{\mathbf{k}}} \frac{1}{i\omega_n - \xi_{\mathbf{k}} - \frac{\Delta_{\mathbf{k}}^2}{i\omega_n + \xi_{\mathbf{k}}}}. \quad (34)$$

Here, as before, $\Delta_{\mathbf{k}}^2 \equiv \Delta_{pg,\mathbf{k}}^2 + \Delta_{sc,\mathbf{k}}^2$. Then, in the same spirit as our derivation of Eq. (10) we exploit the fact that $t_{pg}(P)$ is strongly peaked at small P , which leads us to approximate

$$\overleftrightarrow{P}(Q) \approx 2e^2 \sum_K \frac{\partial \xi_{\mathbf{k}+\mathbf{q}/2}}{\partial \mathbf{k}} \frac{\partial \xi_{\mathbf{k}+\mathbf{q}/2}}{\partial \mathbf{k}} \left[G_K G_{K+Q} + F_{sc,K} F_{sc,K+Q} - F_{pg,K} F_{pg,K+Q} \right] \quad (35)$$

$$\text{where } F_{pg,K} \equiv -\frac{\Delta_{pg,\mathbf{k}}}{i\omega_n + \xi_{\mathbf{k}} + i\gamma} G_K \quad (36)$$

From Eq. (35) and $\text{Re } \sigma^{para}(\Omega) \equiv -\text{Im } P_{xx}(\Omega)/\Omega$ the paramagnetic contribution to the dc conductivity

$$\text{Re } \sigma^{para}(0) \approx -\lim_{\mathbf{q} \rightarrow 0} \text{Im} \sum_K \left[\frac{2e^2}{i\Omega_m} \left(\frac{\partial \xi_{\mathbf{k}}}{\partial k_x} \right)^2 \left(G_K G_{K+Q} - F_{pg,K} F_{pg,K+Q} + F_{sc,K} F_{sc,K+Q} \right) \right]_{i\Omega_m \rightarrow 0^+} \quad (37)$$

In order to be consistent we rewrite Eq. (22), also adding in the usual BCS condensate terms

$$\left(\frac{n_{xx}}{m} \right)_{dia} \approx -2 \sum_K \left(\frac{\partial \xi_{\mathbf{k}}}{\partial k_x} \right)^2 \left[G_K G_{K+Q} - F_{sc,K} F_{sc,K+Q} - F_{pg,K} F_{pg,K+Q} \right]. \quad (38)$$

We can use Eq. (35) to arrive at Eqs. (4) which were presented earlier in the form of a summary. Note that in previous work in the literature⁴⁷⁻⁴⁹ only the first term involving GG was included, which was recognized^{47,49} as inadequate.

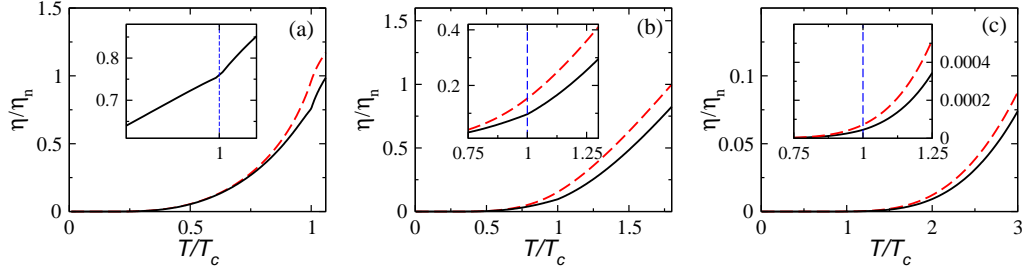


Figure 8: (Color online) Theory plots of shear viscosities as functions of T from BCS to BEC, divided by the counterpart unpaired state viscosities η_n . The red dashed lines are results in absence of explicit bosonic degrees of freedom (associated with the AL diagrams). In (a), $T_c = 0.12T_F$, $T^* = 0.13T_F$ and $1/k_F a = -1$. In (b), $T_c = 0.26T_F$, $T^* = 0.50T_F$ and $1/k_F a = 0$. In (c), $T_c = 0.21T_F$, $T^* = 1.28T_F$ and $1/k_F a = 1$. Expanded plots in different T regimes are shown in the various insets.

E. Proof of Conductivity Sum Rule

We now revisit the issue of compatibility with the important conductivity or transverse sum rule

$$\int_{-\infty}^{\infty} d\Omega \text{Re}\sigma(\Omega) = e^2 (n_{xx}/m)_{dia} \quad (39)$$

in a more general fashion. Here we now include bandstructure effects through the effective mass. Note that we must have two contributions to the conductivity corresponding to the paramagnetic and diamagnetic terms

$$\text{Re}\sigma(\Omega) = -ImP_{xx}(\Omega)/\Omega + \pi\delta(\Omega)[\text{Re}P_{xx}(\Omega) + e^2(n_{xx}/m)_{dia}] \quad (40)$$

Integrating the first term over frequency we find $-\pi\text{Re}P_{xx}(0)$, while the second (delta function) term yields a term $+\pi\text{Re}P_{xx}(0)$, which leaves only the diamagnetic contribution and yields the desired sum rule. Note that this analysis holds both below and above T_c and that *this sum rule is intimately connected to the absence (above T_c) and the presence (below T_c) of a Meissner effect*. Importantly, since $(\frac{n_{xx}}{m})_{dia}$ can be viewed as essentially independent of temperature, when there are approximations in evaluating the transport diagrams, it is appropriate to evaluate the chemical potential μ based on the T -independence in Eq. (38). It should be re-iterated this this diamagnetic contribution is to be distinguished from $n_{eff}(T)$, which enters into the dc transport.

IV. RESULTS FOR VISCOSITY

We now summarize some of our numerical calculations, beginning with the shear viscosity. In Figure. 8 we plot the viscosity divided by a “normal state” value η_n as a function of temperature for $1/k_F a = \pm 1$ and for unitality. This normal state viscosity is to be associated with the (temperature dependent) viscosity of the unpaired state $\eta_n = \int_0^\infty dp \frac{p^6}{15\pi^2 m^2} \left(-\frac{\partial f}{\partial \xi} \Big|_{T^*} \right) \tau_\eta$. In this way we take the same lifetimes in numerator and denominator for the plots, which necessarily cancel out of the ratio. For all $k_F a$, the ratio drops to zero at low temperatures reflecting the decrease in the number of condensate excitations. The red dashed line indicates the behavior when the bosonic excitations are removed and the black solid line shows the full calculated viscosity. Thus, the shaded regions correspond to the contribution from the AL diagrams. This contribution is seen to be largest at unitality, as expanded in the inset to Figure. 8(b). The ratio $\eta(T_c)/\eta_n$ varies from 0.7 to 4.4×10^{-5} as one passes from BCS to BEC in these three cases. At unitality the viscosity at T_c is *reduced by a factor of 10*, relative to the unpaired fluid. A weak signature of the transition is largest in the BCS regime, as shown in the inset to Figure.8(a).

To incorporate trap effects, we begin by summarizing past work on the thermodynamical properties of cold Fermi gases. Counterpart thermodynamical experiments have played a role in characterizing the viscosity^{1,46,59}. Figure 9 presents a comparison of our previous thermodynamical calculations^{5,60} with experiments for both the trapped (left) and homogeneous (right) case. All data is shown in black, while our theoretical results are shown in red. Agreement is reasonably satisfactory in both cases, particularly with the addition of a very small Hartree adjustment which replaces the dashed lines with the solid curves. The first four panels (top and bottom, from the left) correspond to comparisons with the trapped case⁵⁹. The next three are for the homogeneous case with the black lines corresponding to experiments from Japan⁶¹. The third from the left two panels compare the present theory (in red) with these experiments⁶¹ in the upper panel and other analytical (light blue)⁶² as well as Monte Carlo⁶³ (dark blue) calculations in the lower panel. The large scale figure shows that the present approach (red curves) is in quite good

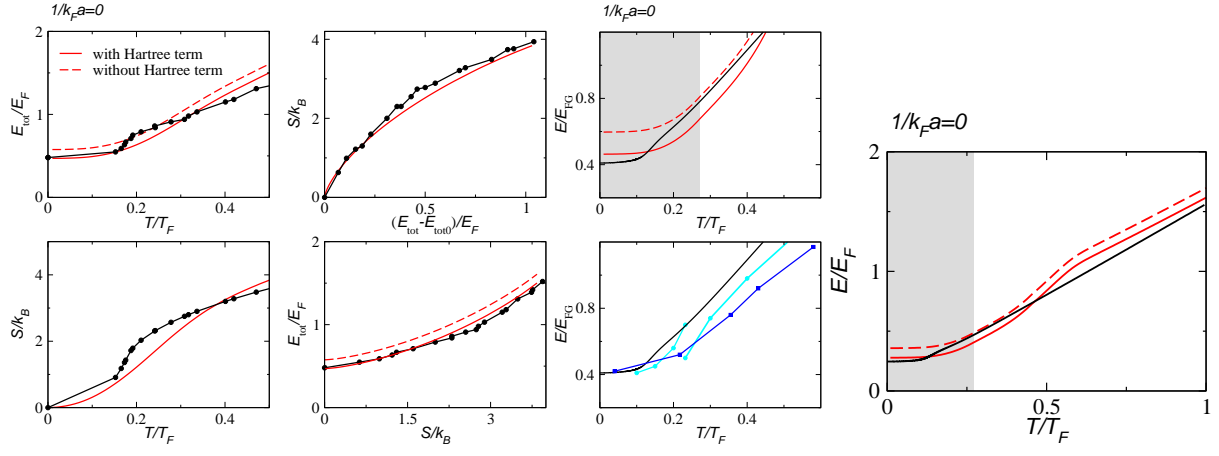


Figure 9: Left: Calculated^{5,60,64} thermodynamical behavior (plotted as red curves, including Hartree shift (solid) and without (dashed)). Results for the trapped case are shown by 4 left panels and for homogeneous case by 3 right panels. Experiments (black lines) on left correspond to those in Ref. 59 and those on right with Ref. 61. Third (lower) panel from left compares E with other theories, one of which shows the usual spurious first order transition⁶⁵ and the other represents Monte Carlo simulations⁶³. Here E_{FG} is defined as in Ref. 65

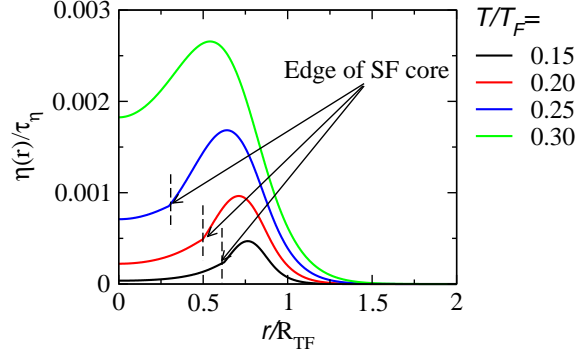


Figure 10: Trap profile for viscosity. The various curves show the shear viscosity as a function of trap position for four different indicated temperatures and R_{TF} is the Thomas-Fermi radius.

agreement with the homogeneous experiments⁶¹ (in black) over a rather wide temperature range. Absent here is the first order transition seen in all other analytic theories.

In Fig. 10 we show the the LDA-calculated viscosity as a function of position in the trap and for various temperatures T . The arrows indicate the edge of the superfluid (SF) core. It can be seen that the viscosity is suppressed in the core region. In this way the nearly-free fermions at the trap edge dominate the trap averaged value for η . As a result the calculated viscosity in a trap is considerably higher than in the homogeneous case.

With these thermodynamical calculations and trap profiles as a backdrop, we now return to an earlier figure, Figure. 6, which addressed comparison of theory and experiment for the shear viscosity. For a unitary Fermi gas, we estimate the transport lifetime from the characteristic broadening of the single particle fermionic spectral function. The latter, in turn, can be found here by fitting^{7,17} Radio Frequency (RF) cold gas experiments. Recall that this fermionic lifetime is associated with a damping contribution in an otherwise BCS-like self energy (conventionally parameterized^{40,41} by “ γ ”). The inset to Figure. 6(a) presents a plot of this RF-deduced lifetime as black circles. The red triangles in this inset represent a plot of the lifetime which one would infer from the data for precise agreement between theory and experiment.

Figure. 6(a) presents a comparison of the viscosity coefficient α between theory (based on the RF-deduced lifetime), as black dots, and experiment⁴⁶ (red triangles) as a function of E . Figure. 6 (b) shows the comparison of η/s where s is the entropy density. We find that η/s appears to be relatively T independent at the lower temperatures. The last figure on the right represents a transcription of the horizontal axis in Figure. 6(b) which plots η/s as a function of temperature, rather than energy E . This is based on using the calculated trap thermodynamics⁵ to rescale the various axes. Moreover, our calculations incorporate the same trap averaging procedure as in Ref. 46. One can anticipate that, particularly at the lower T , the trap-integrated viscosity will be artificially higher than for the homogeneous case, since η will be dominated by unpaired fermions at the trap edge. It

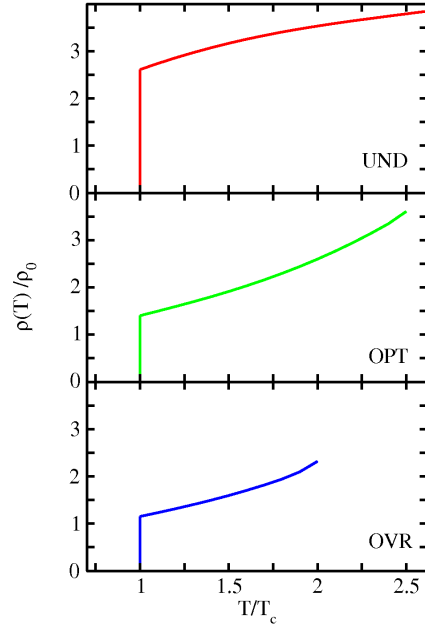


Figure 11: Theoretical plots of resistivity as a function of temperature for three different values of x , corresponding to the pairing onset temperature (or strength of attractive interaction). The UND, OPT and OVR labels as the same as those used in Figure 2, from Reference 31. The resistivity decreases as doping increases, deriving from an increase in the effective carrier number. That the plots stop at temperature $T = T^*$ reflect the fact that Eq. (2) is no longer appropriate when the system is this far from condensation.

should be noted that in the homogeneous case the ratio of the viscosity to its normal counterpart is exponentially activated with T . This is to be contrasted with the behavior of the entropy which reflects bosonic power laws⁵ in T . Overall, it can be seen that our calculations agree favorably with the experimental data. Interestingly, the observed behavior appears more consistent with previous helium-3 experiments²⁶ than those in helium-4²⁹, as can be seen from Figure 1.

V. CONDUCTIVITY IN THE CUPRATES

It is the goal of this section to address the dc conductivity $\sigma(T)$ for a pseudogapped superconductor such as the high T_c cuprates. We approach this problem in a fashion which is analogous to our above discussion of viscosity for an ultracold Fermi gas. In the cuprate literature one associates a fixed stoichiometry (hole doping) with a given excitation gap at T_c , say. The lower the hole doping (x) the larger this gap. Since the parameter x is of no particular interest here, we parameterize instead a given stoichiometry by the size of $\Delta(T_c)$, or alternatively the size of the temperature T^* at which $\Delta(T)$ first vanishes. The two key puzzles of the dc conductivity in the cuprates are the near linearity of the resistivity with temperature and the fact that only the doped holes ($\sigma(T_c) \propto x$) appear to contribute to transport.

A central conclusion of our conductivity study is that, just as for the viscosity, the reduction in the effective carrier number $(n/m(T))_{\text{eff}}$ is revealed to play an important role, both in the T and x dependence of transport. This reduction, in turn, is a consequence of the presence of an excitation gap which persists into the normal phase, and which increases as x decreases. The suppression in the carrier number is substantial relative to the full diamagnetic or sum rule value in Eq. (39). Moreover, $(n/m(T))_{\text{eff}}$ rises nearly monotonically with temperature until T^* . This contribution leads to a non-metallic tendency with σ increasing with T , above T_c . In order to yield a metallic resistivity (which increases with T) the contribution of $(n/m(T))_{\text{eff}}$ must be off-set by taking $\gamma(T)$ to be a higher power than linear. Here we illustrate our results for $T > T_c$ with a Fermi liquid like behavior $\gamma(T/T_c)^2$, which could plausibly be associated with Fermi arcs⁴⁵, which are extended gapless regions due to the smearing out of the d -wave nodes above T_c . This is the most conventional T dependence for transport processes which involve inter-fermion scattering.

We return to Fig.5 (top panel) which was presented earlier and which summarizes the general behavior. Of particular interest is the behavior of the calculated resistivity which is illustrated in Fig.5d which, itself is roughly linear, because of the assumed quadratic or Fermi liquid T^2 dependence in γ . Note that these conductivity calculations are specific to the d -wave case and for an s -wave counterpart, it would be very difficult to find metallic behavior. This can be seen by noting that the inverse viscosity shown in this figure decreases with increasing T , reflecting the even more strongly suppressed carrier number.

Figure 11 presents a more detailed plot of these normal state resistivities for dopings that interpolate between the heavily underdoped (large T^*) and overdoped cases ($T^* \approx T_c$). The resistivities are normalized by the value $\rho_o = \rho(T_c)$ for the case of highest doping. We may characterize each curve, in order of increasing doping, by the ratio $\gamma/\Delta(T_c) = 0.07, 0.20,$ and 0.35 . That the size of the resistivities decreases as one increases the hole concentration, largely reflects the change in gap size and thus in effective carrier number. Indeed, to a first approximation $(n/m(T_c))_{\text{eff}}$ scales close to linearly with x .

Although it is subtle, one can see from the figure that there is a change in the nearly linear slope with increased doping from concave to convex bowing, which may be seen experimentally³¹ in Figure 2. In this way, it would appear that the so-called “optimal” doping (where the bowing is minimal) represents a form of mid-way point, rather than a specific form of “strange metal”⁶⁶.

VI. COMPARISON WITH LITERATURE

A. Pseudogap theories

Since the present transport calculations emphasize the role of the pseudogap, it is useful to clarify the nature of the pseudogap which is specifically associated with BCS-BEC crossover. One of the earliest observations that a pseudogap may be present in BCS-BEC crossover theories is due to Randeria and co-workers⁶⁷. This first generation analysis focused on “spin gap” effects, so that there were a number of claims which are inconsistent with current understanding. Despite statements to the contrary⁶⁷, (i) The pseudogap is not a “spin gap”, but is also to be associated, as we have seen in the present transport calculations, with the “charge channel”. This mirrors the experimental observations⁶⁸ on the nature of the cuprate pseudogap: “It is a quasiparticle gap and not just a spin gap.” (ii) The pseudogap is not associated with “spin-charge” separation above T_c . In this paper (Section III E and Appendix B) we have shown that the absence of a Meissner effect leads to the non-separation of spin-charge degrees of freedom. (iii) The pseudogap in crossover theories is quite distinct from the pseudogap associated with the phase fluctuation scenario (as discussed in Section I B 1).

Our group was one of the earliest (i) To flesh out an understanding of the nature of this pseudogap, and, in particular to show⁶⁹ that the BCS-BEC crossover-pseudogap is not only associated with spin as was claimed⁶⁷, but that more generally it represents a quasi-particle gap. This observation was based on calculations of the fermionic spectral function. (ii) To address gauge invariant electrodynamics in the presence of a pseudogap^{38,56}. (iii) To introduce the concept of a pseudogap into the cold gas literature⁷⁰ and (iv) To introduce⁴⁰ the now widely used expression⁴¹ for the self energy (Eq. (2)).

B. Cold Fermi Gases

There has been a significant effort devoted to reaching a theoretical understanding of the various viscosities associated with highly correlated fermionic superfluids³. A detailed overview exploring the relation between cold atomic gases and hot quark gluon plasmas was presented by Schaefer and Teaney⁷¹. Taylor and Randeria⁷² established sum rules at unitarity for the dynamical counterpart $\eta(\omega)$ and $\zeta_2(\omega)$, which are less general than those in Eqs. (18) and (39). Zwerger and colleagues⁷³ addressed the behavior of the normal unitary gas predicting a minimum in η/s near the superfluid transition.

Bruun and Smith^{47,74} were, perhaps, the first to emphasize the importance of the (static) shear viscosity in cold Fermi gases using both a high temperature fermionic Boltzmann approach and a Kubo-stress tensor based scheme (above T_c), within BCS-BEC theory. They importantly recognized⁴⁷ that the introduction of a pseudogap would lower the normal state η . However, the diagram set which was used was “not conserving”⁴⁷.

Rupak and Schafer⁴ introduced an alternative (bosonic Boltzmann) transport theory in which the low $T \ll T_c$ shear viscosity is dominated by the Goldstone bosons or phonons. They predicted that η/s , increases as temperature decreases. In their approach phonons dominate the low T transport, presumably leading to the same upturn in η , as is seen in helium-4, and shown in Figure 1, on the right. Establishing diagrammatic consistency is a central theme of this paper and within a BCS-like theory the shear viscosity, as a transverse response, does not directly couple¹⁶ to the Nambu-Goldstone bosons. This is to be distinguished from the longitudinal current-current correlations which are the basis for the bulk viscosity and necessarily depend on these collective modes.

C. Transport in High T_c superconductors

Understanding the temperature dependence of the (inverse) conductivity or dc resistivity, particularly near optimal doping, was one of the first puzzles posed by the high temperature superconductors. It should, nevertheless be noted that a number of

ideas and interpretations about transport were established well before there was a full understanding of how widespread was the pseudogap phase (which extends over most of the phase diagram, including optimal doping). For this reason, one can argue that these earlier theories must be reexamined.

A number of different models from spin-charge separation⁶⁶ to marginal Fermi liquid phenomenology⁷⁵ were invoked to explain (i) the unusual normal state temperature power laws observed, *e.g.*, the linear resistivity. A second notable observation (ii) was that the effective carrier number in transport appeared to scale with the number of (extra) doped holes⁶⁶, called x , even though the volume of the Fermi surface scaled as expected with $1 + x$. The first of these experimental observations gave rise to the concept of a distinct “strange metal” phase which was thought to separate the overdoped and underdoped regimes. The second of these gave rise to the concept of “spin-charge” separation. Despite the widespread agreement that the normal state of the cuprates was a non-Fermi liquid phase, there is today a strong belief that the superconducting phase is Fermi liquid based⁶⁶.

It must be noted that the BCS-BEC crossover scenario addresses these issues from a very different perspective. It presumes that there is a smooth evolution, as seen experimentally¹¹ from over to underdoped behavior rather than a distinct strange metal phase near optimal doping. We have argued here that the suppression in the number of carriers may be associated with the fact that the magnitude of the excitation gap grows with underdoping. [In the ac conductivity, this leads to a very small weight for the $\omega \approx 0$ Drude peak, which requires by the sum rule, an additional mid-infrared contribution, now widely observed experimentally²¹.] As noted above, there is no spin-charge separation in the normal phase. Importantly, the superconducting phase has bosonic excitations representing non-condensed pairs (also present above T_c) and therefore this phase is not Fermi liquid based. Finally, the dissipation mechanism here associated with the BCS-BEC crossover scenario arises from the inter-conversion of fermions and pairs, which is distinctly tied to the pseudogap. This is to be distinguished from most transport theories^{76,77} which focus on impurity effects or the dynamics of the pairing boson.

There is a shortcoming in our cuprate transport calculations because we have ignored impurity effects in transport altogether. Away from very low T , it is generally accepted²¹ that they are not particularly important. Nevertheless, they may lead to incomplete condensation^{30,77} in the ground state. Indeed, it is difficult to see how to reconcile claims²¹ that the $T = 0$ superfluid density scales as $\propto x$, with the transverse f-sum rule (Eq. 39)), without invoking incomplete condensation in the ground state. A deeper understanding of a possibly more inhomogeneous treatment of impurities is needed. Fortunately, this is not an issue in the cold gases.

With a growing appreciation for the nature of the pseudogap (and related “Fermi arc” effects), experimentalists have provided some support to our findings. From Ref.78 it is said that “This indicates that the functional form of the dc resistivity of cuprates $\rho_{dc}(T)$ is governed not only by the relaxation processes but also by temperature-dependent numbers of carriers”. Moreover, in Ref.79 it is stated that “One may notice that a natural extension of the present argument would be that the T-linear resistivity usually observed near optimum doping may not necessarily be a sign of a T-linear relaxation rate, because n_{eff} may be changing with T”. An interesting corollary to a carrier number which necessary increases with T , is that the inverse lifetime γ should contain higher powers than linear (we use the most conventional, Fermi liquid dependence $\gamma \propto T^2$) to arrive at metallic behavior for the conductivity.

VII. CONCLUSIONS

In summary, this paper has addressed the role of the pseudogap in the $\omega \rightarrow 0$ conductivity and in the shear viscosity both above and below T_c . We have emphasized the analogy between “bad metals”² and “perfect fluids”¹ seen in high T_c superconductors and the atomic Fermi gases. Both of these phenomena, we argue, may arise from pseudogap effects.

Our approach builds on a consistent gauge invariant treatment of transport (which has not been addressed previously), in which the transverse f-sum rule demonstrably holds. In this paper we have demonstrated success in simultaneously addressing experiments in cold gases and high T_c cuprates within the same transport formalism. As a summary, Figure 5 gives a reasonable understanding of the experiments shown in Figures 3 and 2. Equally important, Figure 6 shows semi-quantitative agreement with shear viscosity data from below to above T_c . We see no sign of the upturn which others have predicted.

It was our intention in this overview to introduce some of the key challenges in understanding transport in the high T_c superconductors to the wider readership interested in perfect fluidity. It is hoped that an appreciation of this broader context may lead to new breakthroughs in understanding superficially distinct, but quite possibly connected, physical systems.

This work is supported by NSF-MRSEC Grant 0820054. We thank Le Luo and John Thomas and T. Mukaiyama, for sharing their data and Benjamin M. Fregoso for helpful conversations. C.C.C. acknowledges the support of the U.S. Department of Energy through the LANL/LDRD Program.

Appendix A: Rewriting the number equation

It is useful to fill in a few steps in the line of argumentation from the text. We wish to show here for the simpler case of a Fermi gas, how the number equation may be rewritten using a Ward identity:

$$P(Q) = \frac{-2e^2}{3m^2} \sum_K (k + \frac{q}{2})^2 [G_K G_{K+Q} + \sum_P t_{pg}(P) G_{0,P-K-Q} G_{0,P-K} G_{K+Q} G_K] \quad (\text{A1})$$

And the number equation

$$\begin{aligned} n &= 2 \sum_K G_K = 2 \sum_K \partial k_\alpha / \partial k_\alpha G_K \\ &= 2 \sum_K k_\alpha G^2(K) \partial G_K^{-1} / \partial k_\alpha \\ &= 2 \sum_K k_\alpha G_K^2 [\partial G_{0,K}^{-1} / \partial k_\alpha - \partial \Sigma(K) / \partial k_\alpha] \\ &= -2 \sum_K k_\alpha G_K^2 [\frac{k_\alpha}{m} - \sum_Q t(Q) \partial G_{0,Q-K}^{-1} / \partial k_\alpha] \\ &= -2 \sum_K k_\alpha G_K^2 [\frac{k_\alpha}{m} + \sum_Q t(Q) G_{0,Q-K}^2 \frac{k_\alpha - q_\alpha}{m}] \\ n &= -\frac{2}{3} \sum_K \frac{k^2}{m} [G_K^2 + \sum_Q t_{pg}(Q) G_{0,Q-K}^2 G_K^2] \end{aligned} \quad (\text{A2})$$

where the last step specializes the result to $T > T_c$. The last equation is the central result we wanted to prove: from which we have

$$K(0) = \frac{ne^2}{m} + P(0) = 0, \quad \text{above } T_c \quad (\text{A3})$$

Appendix B: NSR Theory and the Normal state Structure Factor

In a recent Physical Review Letter¹⁴ we have shown how two photon Bragg scattering can be used to establish *in situ* the presence of coherent order in a superfluid, at any temperature, wavevector and frequency. For the most part experiments on unitary gases have relied on sweeps to the BEC, to find evidence for condensation. Our analysis is based on the definitions and sum rule in Eq. (24). It, thus, depends on imposing the current conservation laws, which have been extensively studied and verified¹⁴.

As an alternate example, here we consider Nozieres Schmitt-Rink (NSR) theory³⁵ in the normal state. Figure 7 indicates the characteristic class of diagrams. These diagrams enter into the density-density and spin-spin correlation functions. The calculations for the spin response build on an earlier publication¹⁷. We define the pair susceptibility $\chi_o(Q) = \sum_P G_{0\uparrow,P} G_{0\downarrow,Q-P}$ where $G_{0\sigma}$ is the bare Green's function. The pair propagator is given by $t_o(Q) = U/(1 + U\chi_o(Q))$, where U is the two-body interaction. Here we present a more systematic discussion of the spin response than what was shown in Sec.III. The interaction term in the Hamiltonian is given by $H_I \sim \int d^3\mathbf{r} J_\mu^S A^{S\mu}$ where $A_\mu^S = (B_z, \mathbf{m})$ is the "effective" 4-vector field and $J_\mu^S = (n^S, \mathbf{J}^S)$. Here B_z is the z component of the magnetic field, \mathbf{m} is the magnetizing field, n^S is the z component of spin and \mathbf{J}^S is the magnetization current. The spin rotational symmetry around the z axis leads to the conservation law of spin: $\partial^\mu J_\mu^S = 0$.

From linear response theory the spin response kernel can be written as

$$Q_{\mu\nu}^S(Q) = \sum_P \lambda_{\mu\sigma}^S(P, P+Q) G_{0\sigma,P+Q} \Lambda_{\nu\sigma}^S(P+Q, P) G_{0\sigma,P} + \frac{n}{m} g_{\mu\nu} (1 - g_{\mu 0}), \quad (\text{B1})$$

where $\lambda_{\mu\sigma}^S(P, P+Q) = (\frac{S_\sigma}{m} (\mathbf{p} + \frac{\mathbf{q}}{2}), S_\sigma)$ is the bare vertex function of the spin-external field interaction, and $\Lambda_{\mu\sigma}^S$ is the full vertex function. There is an implicit summation over the indices σ . Note, importantly, that the vertex function has different signs for different spin indices, which is to be contrasted with the charge or equivalently density response functions. In order to satisfy local conservation laws, the vertex must satisfy a Ward identity: $Q \cdot \sum_P \lambda_{\mu\sigma}^S(P, P+Q) = S_\sigma (G_{0\sigma,P}^{-1} - G_{0\sigma,P+Q}^{-1})$. As

a result, in Nozieres Schmitt-Rink theory there are three contributions $\Lambda_{\sigma}^S = \lambda_{\sigma}^S + \delta\Lambda_{\sigma\text{MT}}^S + \delta\Lambda_{\sigma\text{AL}}^S$, where the subscript MT is associated with the contribution from the Maki-Thompson (MT) like diagrams and AL the Aslamazov-Larkin (AL) diagrams. An important result (for singlet pairing) is that the contribution from the AL diagrams automatically vanishes. Thus, for the spin structure factor $S_S = S_{S0} + S_{\text{MT}_{\text{pg}}^S}$ with $S_{\text{MT}_{\text{pg}}^S} = -S_{\text{MT}_{\text{pg}}^C}$.

By contrast, in the normal state, the dynamical structure factor in NSR theory, for the particle density¹⁷ can be written as the sum $S_C = S_{C0} + S_{\text{MT}_{\text{pg}}^C} + 2S_{\text{AL}}$. Here one should note that $S_{S0} = S_{C0}$. The remaining terms denote the corrections from the MT, and AL diagrams. Note that the spin and charge contributions from the MT term enter with opposite signs. Moreover, the Ward identity implies a cancellation⁶ $S_{\text{MT}_{\text{pg}}^C} + 2S_{\text{AL}} = -S_{\text{MT}_{\text{pg}}^C}$. Thus

$$S_S = S_{S0} + S_{\text{MT}_{\text{pg}}^S} = S_C = S_{C0} - S_{\text{MT}_{\text{pg}}^C}, \quad (\text{B2})$$

which proves the desired result: *in the normal state* the spin and charge degrees of freedom are indistinguishable. Note that the theoretical proof of this result depends on using a consistent theory of BCS-BEC crossover with full gauge invariance. The same diagrams that are used in the above proof are needed to show that there is no Meissner effect in the normal state. In this way we have demonstrated

$$S_{-}(\omega, \mathbf{q}) \equiv 0 \quad \text{above the transition.} \quad (\text{B3})$$

We are now led to an important observation: the quantity $S_{-}(\omega, \mathbf{q})$ for all $\mathbf{q}, \omega, \mathbf{1}/\mathbf{k}_{\text{F}}\mathbf{a}$ can be used as an indication of in-situ superfluid order, without requiring sweeps to the BEC. We show a plot of this behavior in the right side of Figure 7 where it can be seen that the difference structure factor vanishes in the normal state. The behavior below T_c is shown in the figure for the case of BCS-Leggett theory¹⁷.

-
- ¹ J. E. Thomas, Phys. Today **63**, 34 (2010).
 - ² V. J. Emery and S. A. Kivelson, Phys. Rev. Lett. **74**, 3253 (1995).
 - ³ P. K. Kovtun, D. T. Son, and A. O. Starinets, Phys. Rev. Lett. **94**, 111601 (2005).
 - ⁴ G. Rupak and T. Schaefer, Phys. Rev. A **76**, 053607 (2007).
 - ⁵ J. Kinast, A. Turlapov, J. E. Thomas, Q. J. Chen, J. Stajic, and K. Levin, Science **307**, 1296 (2005).
 - ⁶ Q. J. Chen, J. Stajic, S. N. Tan, and K. Levin, Phys. Rep. **412**, 1 (2005).
 - ⁷ Q. Chen, Y. He, C.-C. Chien, and K. Levin, Rep. Prog. Phys. **72** (2010).
 - ⁸ L. P. Kadanoff and P. C. Martin, Annals of Physics **24**, 419 (1963).
 - ⁹ A. J. Leggett, Nature Physics **2**, 134 (2006).
 - ¹⁰ J. T. Stewart, J. P. Gaebler, and D. S. Jin, Nature **454**, 744 (2008).
 - ¹¹ G. Deutscher, A. F. Santander-Syro, and N. Bontemps, Phys. Rev. B **72**, 092504 (2005).
 - ¹² C. Cao, E. Elliot, J. Joseph, H. Wu, J. Petricka, T. Schafer, and J. E. Thomas, Science, 9 December 2010 (10.1126/science.1195219).
 - ¹³ C. C. Chien, H. Guo, Y. He, and K. Levin, Phys. Rev. A **81**, 023622 (2010).
 - ¹⁴ H. Guo, C.-C. Chien, and K. Levin, Phys. Rev. Lett. **105**, 120401 (2010).
 - ¹⁵ H. Guo, D. Wulin, C.-C. Chien, and K. Levin, arXiv:1008.0423.
 - ¹⁶ Y. Nambu, Phys. Rev. **117**, 648 (1960).
 - ¹⁷ C.-C. Chien, Y. He, Q. Chen, and K. Levin, Ann. of Phys. **325**, 214527 (2010).
 - ¹⁸ R. A. Brogliab, A. Molinari, and T. Regge, Ann. Phys. **109**, 349 (1977).
 - ¹⁹ G.M. Bruun and H. Smith, Phys. Rev. A **72**, 043605 (2005); G.M. Bruun and H. Smith, Phys. Rev. A **75**, 043612 (2007).
 - ²⁰ L. Kadanoff and P. Martin, Phys. Rev. **124**, 670 (1961).
 - ²¹ D. N. Basov and T. Timusk, Reviews of Modern Physics **77**, 721 (2005).
 - ²² S. Weinberg, *Gravitation and cosmology* (John Wiley and Sons Inc., New York, USA, 1972).
 - ²³ Y. Ando, in *High Tc superconductors and Related Transition Metal Oxides*, edited by A. Bussmann-Holder and H. Keller (2007), pp. 17–28.
 - ²⁴ O. Valls, and A. Houghton, Phys. Lett. **50A**, 211, (1972); M. A. Shahzamanian, J. Phys. C **21**, 553 (1998).
 - ²⁵ M. Dorfler, H. Brand, and R. Graham, J. Phys. C **13**, 3337 (1980).
 - ²⁶ M. Nakagawa, A. Matsubara, O. Ishikawa, T. Hata, and T. Kodama, Phys. Rev. B **54**, R6849 (1996); C.N. Archie, T.A. Alvesalo, J.D. Reppy, and R.C. Richardson, J. Low Temp. Phys. **42**, 295 (1981).
 - ²⁷ D. Vollhardt, Rev. Mod. Phys. **56**, 99 (1984).
 - ²⁸ L. Roobol, P. Remeijer, S. C. Steel, V. Shumeiko, and G. Frossati, Phys. Rev. Lett. **79**, 685 (1997).
 - ²⁹ A. D. B. Woods and A. C. Hollis Hallet, Can. J. Phys. **41**, 596 (1963).
 - ³⁰ J. Orenstein, in *Handbook of high Temperature superconductors: theory and experiment*, edited by J. R. Schrieffer and J. S. Brooks (2006), p. 299.
 - ³¹ A. F. Santander-Syro, R. P. S. M. Lobo, and N. Bontemps, Phys. Rev. B **70**, 134504 (2004).
 - ³² T. Timusk and B. Statt, Rep. Prog. Phys. **62**, 61 (1999).
 - ³³ A. J. Leggett, in *Modern Trends in the Theory of Condensed Matter* (Springer-Verlag, Berlin, 1980), pp. 13–27.

- ³⁴ D. M. Eagles, Phys. Rev. **186**, 456 (1969).
- ³⁵ P. Nozières and S. Schmitt-Rink, J. Low Temp. Phys. **59**, 195 (1985).
- ³⁶ C. C. Chien, Q. J. Chen, and K. Levin, Phys. Rev. A **78**, 043612 (2008).
- ³⁷ W. S. Lee, I. M. Vishik, K. Tanaka, D. H. Lu, T. Sasagawa, N. Nagaosa, T. P. Devereaux, Z. Hussain, and Z. X. Shen, Nature **450**, 81 (2007).
- ³⁸ I. Kosztin, Q. J. Chen, B. Jankó, and K. Levin, Phys. Rev. B **58**, R5936 (1998).
- ³⁹ V. J. Emery and S. A. Kivelson, Nature **374**, 434 (1995).
- ⁴⁰ J. Maly, Ph.D. thesis, University of Chicago (1996), (unpublished).
- ⁴¹ M. R. Norman, M. Randeria, H. Ding, and J. C. Campuzano, Phys. Rev. B **57**, R11093 (1998).
- ⁴² M. R. Norman, A. Kanigel, M. Randeria, U. Chatterjee, and J. C. Campuzano, Phys. Rev. B **76**, 174501 (2007).
- ⁴³ Q. J. Chen and K. Levin, Phys. Rev. B **78**, 020513(R) (2008).
- ⁴⁴ Q. J. Chen and K. Levin, Phys. Rev. Lett. **102**, 190402 (2009).
- ⁴⁵ A. Kanigel, M. R. Norman, M. Randeria, U. Chatterjee, S. Souma, A. Kaminski, H. M. Fretwell, S. Rosenkranz, M. Shi, T. Sato, et al., Nature Phys. **2**, 447 (2006).
- ⁴⁶ A. Turlapov, J. Kinast, B. Clancy, L. Luo, J. Joseph, and J. E. Thomas, J. Low Temp. Phys. **150**, 567 (2008).
- ⁴⁷ G. M. Bruun and H. Smith, Phys. Rev. A **75**, 043612 (2007).
- ⁴⁸ M. F. Smith and R. H. McKenzie, Phys. Rev. B **82**, 012501 (2010).
- ⁴⁹ A. Levchenko, T. Micklitz, M. R. Norman, and I. Paul, Phys. Rev. B **82**, 060502(R) (2010).
- ⁵⁰ L. P. Kadanoff and P. C. Martin, Phys. Rev. **124**, 670 (1961).
- ⁵¹ B. R. Patton, Phys. Rev. Lett. **27**, 1273 (1971).
- ⁵² E. Abrahams and T. Tsuneto, Phys. Rev. **152**, 416 (1966).
- ⁵³ J. Maly, B. Jankó, and K. Levin, Physica C **321**, 113 (1999).
- ⁵⁴ J. Maly, B. Jankó, and K. Levin, Phys. Rev. B **59**, 1354 (1999).
- ⁵⁵ I. Kosztin, Q. J. Chen, Y.-J. Kao, and K. Levin, Phys. Rev. B **61**, 11662 (2000).
- ⁵⁶ Q. J. Chen, I. Kosztin, B. Jankó, and K. Levin, Phys. Rev. Lett. **81**, 4708 (1998).
- ⁵⁷ K. Levin, Q. J. Chen, C. C. Chien, and Y. He, Ann. Phys. **325**, 233 (2010).
- ⁵⁸ M. Randeria, in *Bose Einstein Condensation*, edited by A. Griffin, D. Snoke, and S. Stringari (Cambridge Univ. Press, Cambridge, 1995), pp. 355–92.
- ⁵⁹ L. Luo and J. E. Thomas, J. Low Temp. Phys. **154**, 1 (2009).
- ⁶⁰ Y. He, C.-C. Chien, Q. J. Chen, and K. Levin, Phys. Rev. B **76**, 224516 (2007).
- ⁶¹ M. Horikoshi, S. Nakajima, M. Ueda, and T. Mukaiyama, Science **327**, 442 (2010).
- ⁶² H. Hu, X.-J. Liu, and P. D. Drummond, Phys. Rev. A **77**, 061605(R) (2008).
- ⁶³ A. Bulgac, J. Drut, and P. Magierski, Phys. Rev. Lett. **96**, 090404 (2006).
- ⁶⁴ Q. J. Chen, J. Stajic, and K. Levin, Phys. Rev. Lett. **95**, 260405 (2005).
- ⁶⁵ H. Hu, X. J. Liu, and P. D. Drummond, Europhys. Lett. **74**, 574 (2006).
- ⁶⁶ P. A. Lee, N. Nagaosa, and X. G. Wen, Rev. Mod. Phys. **78**, 17 (2006).
- ⁶⁷ M. Randeria, in *Models and Phenomenology for Conventional and High-temperature Superconductivity*, edited by G. Iadonisi, J. R. Schrieffer, and M. L. Chialfalo, Società Italiana di Fisica Bologna, Italy (IOS Press, 1998), vol. 136 of *Proc. Int'l School of Physics "Enrico Fermi" Courses*, pp. 53–75.
- ⁶⁸ M. Sutherland, D. Hawthorn, R. Hill, F. Ronning, H. Zhang, E. Boaknin, M. Tanatar, J. Paglione, R. Liang, D. Bonn, et al., Physica C **408-410**, 672 (2004).
- ⁶⁹ B. Jankó, J. Maly, and K. Levin, Phys. Rev. B **56**, R11407 (1997).
- ⁷⁰ J. Stajic, J. N. Milstein, Q. J. Chen, M. L. Chiofalo, M. J. Holland, and K. Levin, Phys. Rev. A **69**, 063610 (2004).
- ⁷¹ T. Schaefer and D. Teaney, Rep. Prog. Phys. **72**, 126001 (2009).
- ⁷² E. Taylor and M. Randeria, Phys. Rev. A **81**, 053610 (2010).
- ⁷³ T. Enss, R. Haussmann, and W. Zwerger, arXiv:1008.0007.
- ⁷⁴ G. M. Bruun and H. Smith, Phys. Rev. A **72**, 043605 (2005).
- ⁷⁵ C. M. Varma, P. B. Littlewood, S. Schmitt-Rink, E. Abrahams, and A. E. Ruckenstein, Phys. Rev. Lett. **63**, 1996 (1989).
- ⁷⁶ S. Quinlan, P. Hirschfeld, and D. Scalapino, Phys. Rev. B **53**, 8575 (1996).
- ⁷⁷ P. Lee, Phys. Rev. Lett. **71**, 1887 (1993).
- ⁷⁸ Y. S. Lee, K. Segawa, Z. Q. Li, W. J. Padilla, M. Dumm, S. V. Dordevic, C. C. Homes, Y. Ando, and D. N. Basov, Phys. Rev. B. **72**, 054529 (2005).
- ⁷⁹ Y. Ando, Y. Kunta, S. Komiya, S. Ono, and K. Segawa, Phys. Rev. Lett. **92**, 197001 (2004).